

# Structural basis for intrinsic transcription termination

<https://doi.org/10.1038/s41586-022-05604-1>

Received: 18 August 2022

Accepted: 25 November 2022

Published online: 11 January 2023

 Check for updates

Linlin You<sup>1,2</sup>, Expery O. Omollo<sup>3</sup>, Chengzhi Yu<sup>1,2</sup>, Rachel A. Mooney<sup>3</sup>, Jing Shi<sup>4,5</sup>, Liqiang Shen<sup>1,2</sup>, Xiaoxian Wu<sup>1,2</sup>, Aijia Wen<sup>4</sup>, Dingwei He<sup>1,2</sup>, Yuan Zeng<sup>1,2</sup>, Yu Feng<sup>4</sup>✉, Robert Landick<sup>3</sup>✉ & Yu Zhang<sup>1</sup>✉

Efficient and accurate termination is required for gene transcription in all living organisms<sup>1,2</sup>. Cellular RNA polymerases in both bacteria and eukaryotes can terminate their transcription through a factor-independent termination pathway<sup>3,4</sup>—called intrinsic termination transcription in bacteria—in which RNA polymerase recognizes terminator sequences, stops nucleotide addition and releases nascent RNA spontaneously. Here we report a set of single-particle cryo-electron microscopy structures of *Escherichia coli* transcription intrinsic termination complexes representing key intermediate states of the event. The structures show how RNA polymerase pauses at terminator sequences, how the terminator RNA hairpin folds inside RNA polymerase, and how RNA polymerase rewinds the transcription bubble to release RNA and then DNA. These macromolecular snapshots define a structural mechanism for bacterial intrinsic termination and a pathway for RNA release and DNA collapse that is relevant for factor-independent termination by all RNA polymerases.

Genomic DNA is composed of functional genes that are transcribed to RNAs with defined 5' and 3' boundaries. The 5' boundary is defined by a promoter, from which RNA polymerase (RNAP) initiates RNA synthesis<sup>5</sup>. The 3' boundary is defined by a terminator, at which RNAP stops transcription and releases the nascent RNA<sup>1,2,6,7</sup>. Efficient and accurate termination is required for gene transcription in all living organisms to ensure precise control of transcription units and to define the 3' boundary of RNA transcripts<sup>1,2</sup>. Programmed transcription termination of RNAP occurs by two pathways, factor-independent (also called intrinsic) and factor-dependent termination. Intrinsic termination requires only interactions of RNA and DNA with RNAP and can be modulated by transcription factors<sup>3,4,7,8</sup>. Intrinsic termination is prevalent in viruses and bacteria and is used in eukaryotes by RNAPIII<sup>3,4,9</sup>.

The intrinsic terminator sequences in bacteria comprise a GC-rich inverted repeat immediately followed by a stretch of thymidine that encodes an RNA with a GC-rich terminator hairpin immediately followed by a uridine tract<sup>10,11</sup>. Genetic, biochemical and single-molecule studies all suggest that intrinsic termination occurs via three sequential intermediates: (1) a pause state when RNAP pauses at the terminator in response to the rU–dA hybrid and preceding G-rich sequence that are thought to inhibit tDNA translocation<sup>12–14</sup>; (2) a hairpin-nucleation state when the RNA hairpin partially folds into RNAP; and (3) a hairpin-completion state when the RNA hairpin completes folding and releases nascent RNA aided by the weak rU–dA base pairs. However, how the compact terminator sequence pauses, destabilizes and dissociates RNAP remains unknown. Here we determined a set of cryo-electron microscopy (cryo-EM) structures representing the key intermediate states formed during intrinsic termination.

## RNAP pauses at the terminator sequence

RNAP first pauses at the –2 or –1 position (–1 corresponds to the eighth RNA nucleotide after the terminator hairpin) of intrinsic terminators independent of the terminator hairpin to begin intrinsic termination<sup>4,12</sup>. To study the structural mechanism of the terminator-induced pause, we reconstituted a paused transcription termination complex (TTC pause) using the *E. coli* RNAP core enzyme and a nucleic acid scaffold that comprises a nascent RNA with a  $\lambda_{t_{R2}}$  terminator sequence but lacking the upstream half of the hairpin stem (Fig. 1a). We determined the TTC-pause structure at 3.6 Å resolution using single-particle cryo-EM (Extended Data Fig. 1 and Extended Data Table 1). The cryo-EM map of TTC pause shows unambiguous signals for ribonucleotides and deoxyribonucleotides within and near the transcription bubble, including the 10-base-pair (bp) RNA–DNA hybrid, the 10-nucleotide (nt) single-stranded non-template DNA (ntDNA), the 12-bp downstream double stranded DNA (dsDNA), and 3 bp of the upstream dsDNA (Fig. 1b,c, Extended Data Fig. 1h and Supplementary Video 1).

The RNA–DNA hybrid of TTC pause adopts a half-translocated state, an off-pathway state that has been reported previously in paused transcription complexes<sup>13–15</sup> and differs from the post-translocated state seen in elongation complexes reconstituted on similar scaffolds with non-pause sequences<sup>16</sup>. In the half-translocated state, the RNA strand has translocated by one nucleotide from the pre-translocation state but the next template strand DNA (tDNA) nucleotide remains base-paired in the downstream dsDNA (Fig. 1d, Extended Data Fig. 2c and Supplementary Video 1). This base pair is unwound and untranslocated except for a slight positional shift of backbone phosphates (Extended Data Fig. 2c).

<sup>1</sup>Key Laboratory of Synthetic Biology, CAS Center for Excellence in Molecular Plant Sciences, Shanghai Institute of Plant Physiology and Ecology, Chinese Academy of Sciences, Shanghai, China. <sup>2</sup>University of Chinese Academy of Sciences, Beijing, China. <sup>3</sup>Department of Biochemistry and Department of Bacteriology, University of Wisconsin-Madison, Madison, WI, USA. <sup>4</sup>Department of Biophysics, and Department of Infectious Disease of Sir Run Run Shaw Hospital, Zhejiang University School of Medicine, Hangzhou, China. <sup>5</sup>Department of Pathogen Biology, School of Medicine and Holistic Integrative Medicine, Nanjing University of Chinese Medicine, Nanjing, China. ✉e-mail: yufengjay@zju.edu.cn; rlandick@wisc.edu; yzhang@cemps.ac.cn

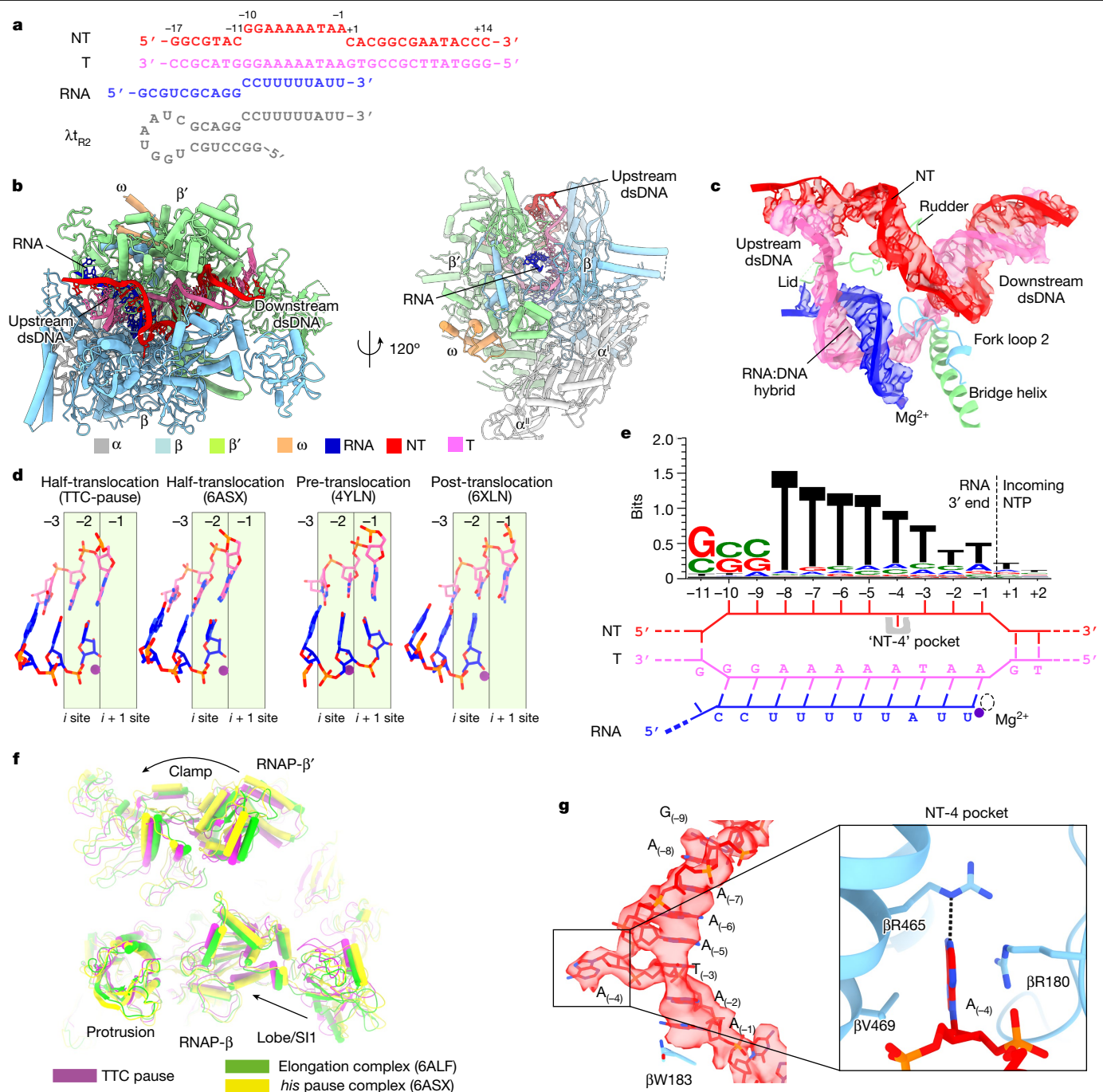


**Fig. 1 | The TTC-pause complex.** **a**, Sequences of the nucleic acid scaffold used in the cryo-EM study. The potential hairpin-forming nucleotides of the nascent RNA are highlighted in bold. The natural λt<sub>R2</sub> sequence is shown in grey for comparison. **b**, The structural model of TTC pause in front and side views. **c**, The cryo-EM map of the nucleic acid scaffold. **d**, Comparison of RNA-DNA translocation states in the TTC-pause complex, the half-translocation state in a hairpin-stabilized paused transcription elongation complex (*his*PEC; Protein Data Bank (PDB): 6ASX), a pre-translocation complex (PDB: 4YLN), and a

post-translocation complex (PDB: 6XLN). **e**, The consensus sequence of bacterial intrinsic terminators<sup>11</sup> (top) and schematic presentation of the nucleotides of the transcription bubble in the TTC-pause complex (bottom). **f**, Conformational comparison of the TTC-pause complex, the transcription elongation complex (TEC; PDB: 6ALF) and *his*PEC (PDB: 6ASX). **g**, Left, cryo-EM map and structural model of the ntDNA of the transcription bubble. Right, expanded view of the interaction between the flipped A<sub>(-4)</sub> nucleotide and the NT-4 pocket.

Half-translocation results in a tilted RNA-DNA hybrid and an empty NTP-binding site (*i* + 1 site) lacking the template nucleotide for base pairing to the incoming NTP (Fig. 1d). A survey of 100 native intrinsic terminators shows that intrinsic terminators resemble the consensus sequence for elemental pausing at two out of the three key positions<sup>11,17,18</sup> (S<sub>-10</sub>U<sub>-1</sub> versus S<sub>-10</sub>Y<sub>-1</sub>G<sub>+1</sub>; Fig. 1e and Extended Data Fig. 2a, b). We infer that the sequences at the upstream and downstream edges of

the transcription bubble (S<sub>-10</sub>, U<sub>-1</sub>) probably account for the formation of the half-translocated conformation of the TTC-pause complex by inhibiting tDNA translocation<sup>16,19</sup>.

We also observed a global conformational change of RNAP involving multiple structural modules in TTC pause compared with the normal transcription elongation complex<sup>16</sup>. The clamp module of RNAP rotates along an axis parallel to the bridge helix. The rotation movement

of clamp module resembles the ‘swivel’ movement observed in the hairpin-stabilized paused elongation complex<sup>13,14,19</sup> (PEC), but it only reaches halfway to the fully swivelled position (Fig. 1f). However, distinct from the swivel movement in the hairpin-stabilized PEC complex, the RNAP  $\beta$  lobe–sequence insertion 1 (SI1) module in TTC pause moves slightly towards the RNAP main cleft, probably owing to unique interactions between RNAP and ntDNA of the transcription bubble (Fig. 1g and Supplementary Video 1). These movements of the structural modules in TTC pause probably accommodate the slightly shifted downstream dsDNA in the downstream dsDNA channel and stabilize the half-translocated RNA–DNA hybrid in the main cleft (Extended Data Fig. 2c,d).

The cryo-EM map of TTC pause revealed a novel path of the single-stranded ntDNA in the transcription bubble across the RNAP main cleft. The ntDNA was accommodated in the upper floor of the main cleft and was separated from the active site tunnel by the RNAP- $\beta'$  rudder loop and fork loop 2 (Fig. 1c and Extended Data Fig. 2e). Eight nucleotides of the ntDNA form a continuous base stack that starts upstream at the RNAP  $\beta'$  coiled-coil (Fig. 1g and Extended Data Fig. 2e), travels across the cleft to the RNAP  $\beta$  protrusion and lobe, and follows fork loop 2 to reach the downstream dsDNA (Extended Data Fig. 2e). The –4 adenine is flipped out approximately 180° from this continuous base stack. The backbone phosphates of the stacked nucleotides are stabilized by polar contacts with RNAP residues  $\beta'$  R271,  $\beta'$  R297,  $\beta$  R470 and  $\beta$  R473; residue  $\beta$  W183 supports the 8-nt base stack and separates it from the downstream dsDNA (Extended Data Fig. 2f). We anticipate similar interactions between RNAP and the natural ntDNA in a complementary transcription bubble because the protein–DNA interactions are not sequence-specific.

The flipped out –4 nucleotide inserts into a protein pocket (NT–4 pocket) located in the gap between the RNAP  $\beta$  protrusion and lobe (Fig. 1g). A pyrimidine base was also found occupying the same pocket in previously reported structures<sup>20</sup>, suggesting that the pocket accommodates bases without sequence specificity. In our structure, the A–4 base was sandwiched between residues  $\beta$  R180 and  $\beta$  V469. The N1 atom of the adenine moiety makes a hydrogen bond with  $\beta$  R465 (Fig. 1g and Extended Data Fig. 2f). To test for potential effects of the pocket interaction on intrinsic termination, we measured the termination efficiency of RNAP derivatives bearing substitutions in the pocket at three different terminators. The results revealed no obvious effects on termination efficiency of disruption of either the stacking interaction ( $\beta$  R180A– $\beta$  V469A) or the hydrogen-bond interaction ( $\beta$  R465A) (Extended Data Fig. 3a–f). Disruption of the pocket interaction also had no effect on transcriptional pausing at a hairpin-less  $\lambda$ P<sub>R</sub> terminator (Extended Data Fig. 3g). Although no significant role in intrinsic termination was found, the pocket interaction might have roles in other stages of transcription<sup>20</sup>.

## An RNA hairpin forms in the RNA exit channel

The RNA hairpin of intrinsic terminators is thought to begin folding in the RNA exit channel when RNAP pauses at terminators, a stage called hairpin nucleation<sup>12,21</sup>. To trap the hairpin-nucleation complex of transcription termination (TTC hairpin), we incubated the TTC-pause complex with a 10-nt antisense RNA (asRNA10) to form a 10-bp RNA duplex with the nascent RNA that mimics the upstream part of the hairpin stem (–20 to –11) and determined a TTC-hairpin structure at 3.1 Å resolution (Fig. 2a, Extended Data Fig. 4 and Extended Data Table 1). The cryo-EM map of TTC hairpin revealed clear and sharp signals for the transcription bubble. The RNA–DNA hybrid adopts the same half-translocated conformation as in TTC pause and the ntDNA nucleotides stack together and make interactions with RNAP essentially as in TTC pause (Fig. 2c and Extended Data Fig. 5a). The cryo-EM map of TTC hairpin shows unambiguous signal for the 14-bp downstream dsDNA, the 4-bp upstream dsDNA and, notably, the 10-bp dsRNA in

the RNA exit channel (Fig. 2b,c, Extended Data Fig. 4e and Supplementary Video 2). These features indicate that we successfully trapped the TTC-hairpin complex of intrinsic termination.

The 10-bp dsRNA was tightly accommodated in the RNA exit channel by the RNAP  $\beta'$  dock, the  $\beta$  C-terminal helix region ( $\beta$  CTR), the  $\beta'$  zinc-binding domain ( $\beta'$  ZBD), and the  $\beta$  flap (Fig. 2d), consistent with the important roles of these elements in intrinsic termination<sup>22,23</sup>. The phosphate backbones of the RNA hairpin were held by RNAP polar residues in the RNA exit channel, including  $\beta'$  K66,  $\beta'$  K76,  $\beta'$  R77,  $\beta$  Q1256,  $\beta'$  K395,  $\beta'$  K398,  $\beta$  N856,  $\beta$  K890,  $\beta$  K914 and  $\beta$  R919 (Fig. 2e). The innermost base pair of the RNA duplex reaches the bottom of the RNA exit channel. The –11G of the nascent RNA makes a base-stack interaction with  $\beta$  L1253 and the sugar moiety of the asRNA –11C fits into a shallow pocket of  $\beta'$  ZBD (Fig. 2f). The RNA duplex in our structure of TTC hairpin lacks the ssRNA upstream of the hairpin stem, which can be routed out of the RNA exit channel through a positively charged groove without interfering with the hairpin stem in the RNA exit channel (Extended Data Fig. 5b). Further extension of the RNA hairpin stem into the active centre cleft was stopped by  $\beta$  Sw3,  $\beta'$  ZBD, and  $\beta'$  lid (Fig. 2g). Most of these features of the hairpin stem closely match those observed for the hairpin-stabilized PEC (hisPEC), even though the TTC hairpin stem is extended 1 bp closer to the RNA–DNA hybrid<sup>13,14</sup>.

The formation of an RNA duplex in TTC hairpin causes a global conformational change of RNAP. The RNA duplex enlarges the RNA exit channel by stretching the four surrounding structural elements (Fig. 2h), probably triggering a global conformational change of RNAP structure modules, including further swivelling of the clamp module and outward rotation of the protrusion and lobe module (Fig. 2i and Supplementary Video 2). The net result of such global rearrangement widens the main cleft and secures the hairpin in the RNA exit channel. Moreover, the fully swivelled conformation prevents the trigger loop from refolding and further stabilizes the half-translocated RNA–DNA hybrid<sup>13,24</sup>. In short, our TTC-hairpin structure shows that the RNA duplex in the RNA exit channel induces further conformational changes of RNAP compared with TTC pause to inhibit nucleotide addition, stabilize the pause, and probably to prepare for the subsequent completion of the RNA hairpin.

The completion of the RNA hairpin requires melting of at least two upstream base pairs of RNA–DNA hybrid<sup>25</sup>. Our cryo-EM structure of TTC hairpin provides a structural clue for how the first base pair of the RNA–DNA hybrid is disrupted. In the TTC-hairpin structure, the half-translocated RNA–DNA hybrid shifts each template nucleotide towards upstream from their respective positions in the pre-translocation state (Fig. 2j). As a result, the –10 nucleotide of tDNA shifts approximately 1 bp out of the RNAP active centre cleft to a new position under the small tunnel formed by the rudder and lid loops (Fig. 2k and Extended Data Fig. 5c,d). This new location enables unpairing of tDNA with the –10 nucleotide of the nascent RNA and its flipping through the tunnel to pair with the –10 nucleotide of ntDNA (Extended Data Fig. 5e and Supplementary Video 3). Rewinding of this upstream base pair of the transcription bubble would weaken the next base pair in the RNA–DNA hybrid owing to the loss of stacking interactions, thus enabling its disruption and lowering the energy barrier to RNA hairpin completion. The base pair at the –10 position shows the weakest map signals among the nucleotides of the RNA–DNA hybrid (Extended Data Fig. 5f), indicative of its high flexibility, which is necessary for spontaneous unwinding.

## DNA rewinding promotes RNA release

The last stage of transcription termination involves disruption of the RNA–DNA hybrid, completion of the RNA hairpin, rewinding of the transcription bubble and release of RNA and DNA<sup>4,12,25–28</sup>. To trap intermediates of the last stage of intrinsic termination, we took advantage of asRNA-induced termination<sup>4</sup> (Fig. 3a). The in vitro transcription

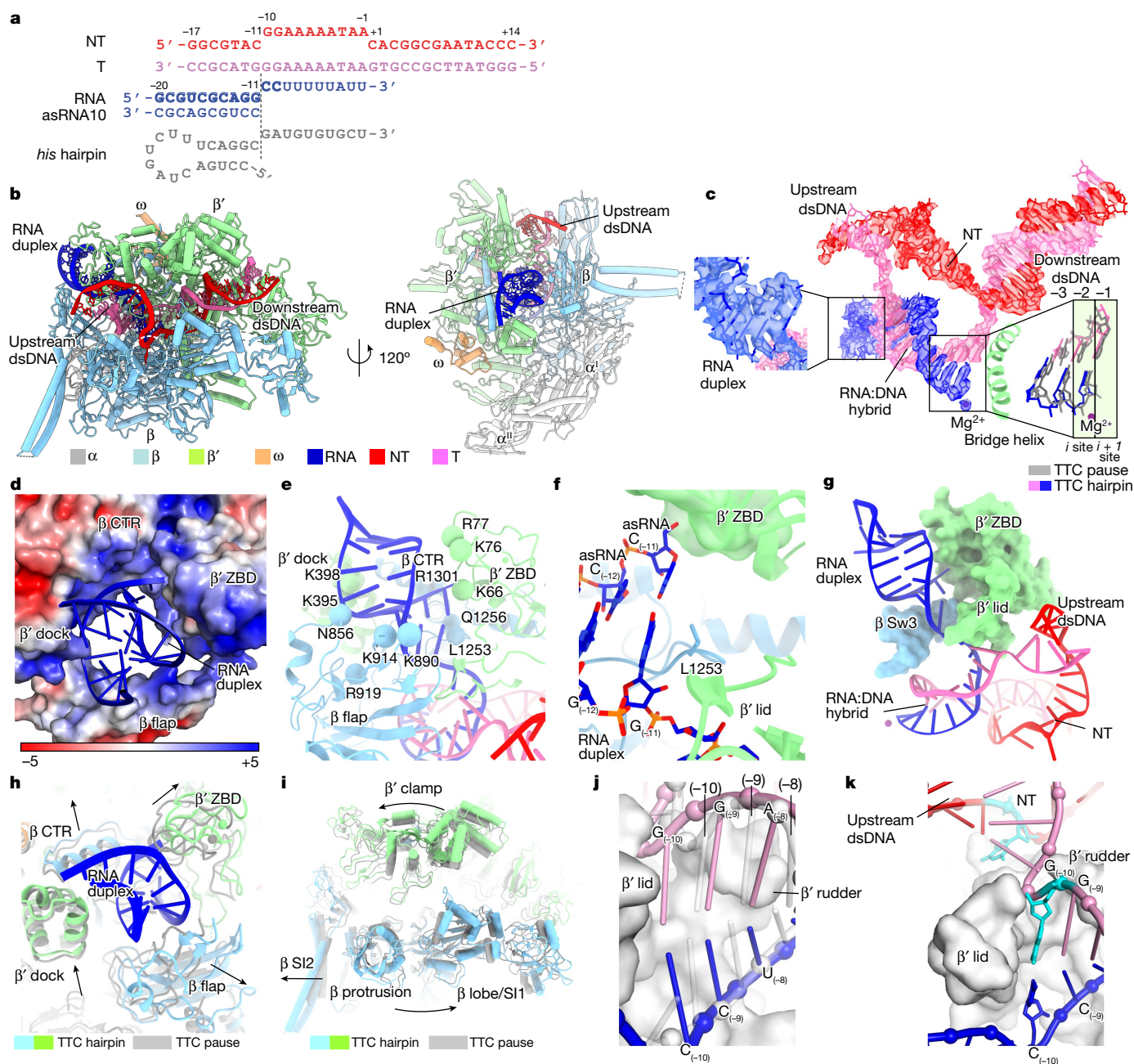


**Fig. 2 | The TTC-hairpin complex.** **a**, The nucleic acid scaffold and the antisense RNA (asRNA) used for cryo-EM structure determination. The potential hairpin-forming nucleotides of the nascent RNA are highlighted in bold. The dashed line defines the downstream edge of the RNA duplex in the TTC hairpin. The *his* hairpin is shown as a comparison. **b**, The structural model of TTC hairpin in front and side views. **c**, Cryo-EM map of the nucleic acid scaffold. Left, an expanded view of the map for the RNA duplex in the RNA exit channel. Right, superimposition of base pairs -3 to -1 of the RNA-DNA hybrid between TTC hairpin and TTC pause (grey). **d**, The RNA duplex in the RNA exit channel. The electrostatic potential surface of RNAP was generated using APBS tools in Pymol. **e**, Detailed interactions of the RNA duplex with residues in the RNA exit channel. The C $\alpha$  atoms of polar residues within hydrogen-bonding

distance of the phosphate backbone of the RNA duplex are shown as spheres. **f**, The interaction of the -11 base pair of the RNA duplex with residues in the RNA exit channel. **g**, Further extension of the RNA duplex is blocked by the RNAP  $\beta'$  ZBD,  $\beta'$  lid and  $\beta$  Sw3 motifs. **h**, Structural comparison of the RNA exit channel between TTC pause and TTC hairpin. **i**, The global conformational difference between TTC hairpin and TTC pause. **j**, Comparison of the first three base pairs of the RNA-DNA hybrid between TTC hairpin (pink and blue) and TEC (grey) (PDB: 6ALF). The two structures are superimposed on the basis of the RNAP  $\beta'$  lid and rudder motifs. **k**, The -10 guanine of the tDNA is under the tunnel formed by RNAP  $\beta'$  lid and rudder and ready to pair with the -10 nucleotide of ntDNA.

termination assay suggests that, upon challenge with asRNA12 that could form an RNA duplex with nascent RNA mimicking RNA hairpin completion, RNAP began to release nascent RNA within 30 s and released most of the nascent RNA at 5 min (Fig. 3b). Therefore, we challenged the TTC-pause complex with an excess amount of 12-nt asRNA

and vitrified the reaction mixture after 3 min of incubation, followed by cryo-EM data collection. We reconstructed a cryo-EM map at 3.5 Å resolution from 54,471 particles (19% of total particles) after two rounds of 3D classification (Extended Data Fig. 6 and Extended Data Table 1). The cryo-EM density map for this complex (TTC release) shows clear

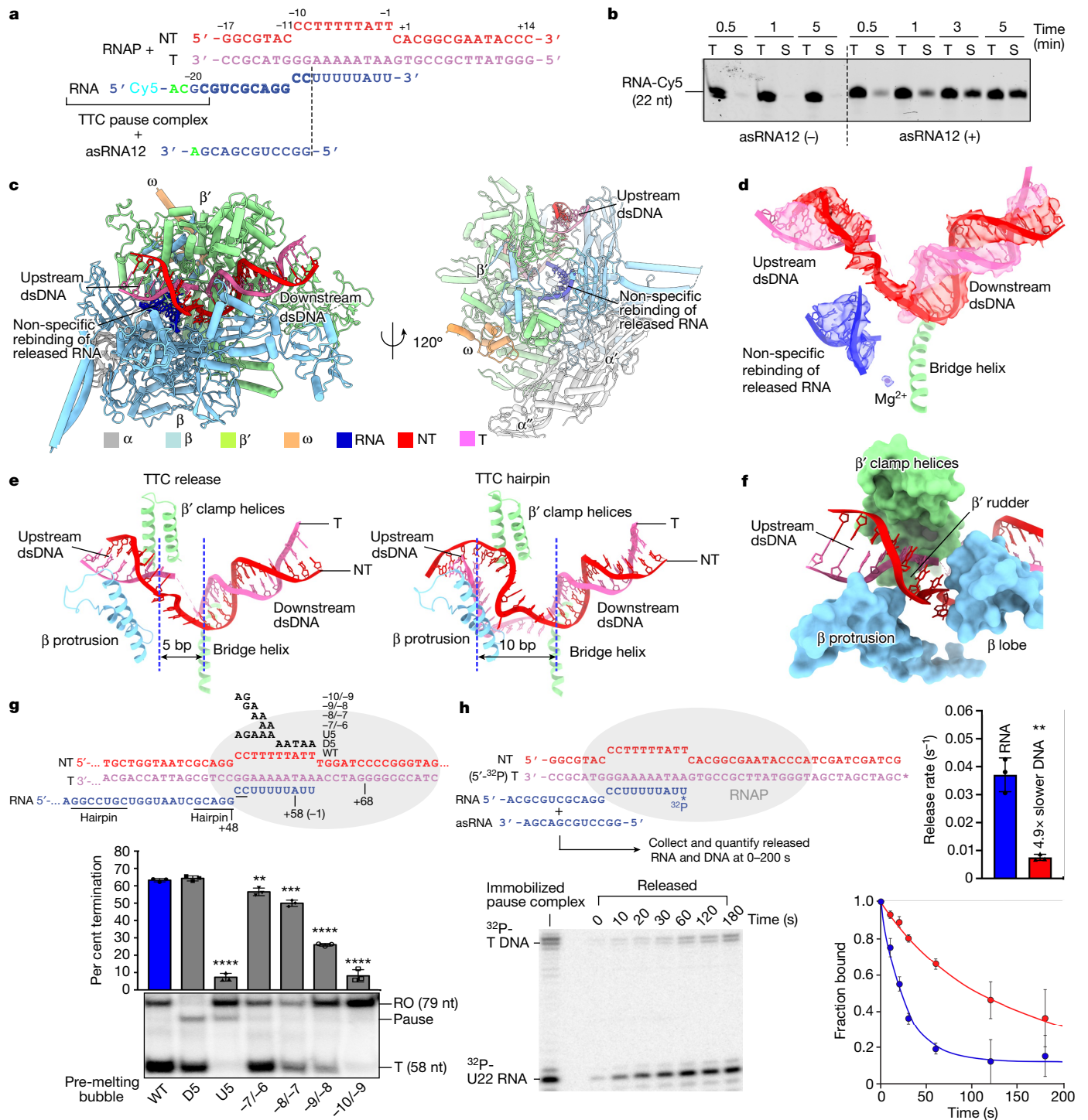


**Fig. 3 | The release complex of transcription termination. a**, The asRNA-induced termination strategy used to obtain the cryo-EM structure of TTC release. The potential hairpin-forming nucleotides of the nascent RNA are highlighted in bold. The dashed line defines the downstream edge of the RNA duplex. asRNA12, 12-nt asRNA. **b**, The results of the RNA release assay show that asRNA12 induces release of nascent RNA in a time-dependent manner. The experiment was repeated three times independently with similar results. Raw gel data are presented in Supplementary Fig. 1e. T, total fraction; S, supernatant fraction. **c**, The structural model of TTC release in front and side views. **d**, Cryo-EM map and model of the nucleic acid scaffold in TTC release. **e**, The comparison of transcription bubble sizes in TTC release and TTC hairpin. **f**, The reword 5-bp dsDNA (-10 to -6) is loosely restrained by the  $\beta$  protrusion, the

$\beta'$  clamp helices and the  $\beta'$  rudder and further rewinding of the upstream dsDNA is stopped by the  $\beta$  lobe domain owing to a closed clamp. **g**, In vitro transcription assay suggests that DNA rewinding is required for intrinsic termination at the  $\lambda t_{r2}$  terminator. Data are mean  $\pm$  s.d.,  $n = 3$  independent experiments. Two-tailed unpaired  $t$ -tests. Raw gel data are shown in Supplementary Fig. 1f. **h**, RNA is released from TTC during termination more quickly than DNA. A TTC scaffold making all RNAP contacts, labelled with <sup>32</sup>P in the template strand 5' phosphate and RNA 3' phosphodiester, was immobilized on beads. Upon asRNA addition, the rate of RNA release was  $0.037 \pm 0.006 \text{ s}^{-1}$  whereas DNA was released at  $0.0075 \pm 0.001 \text{ s}^{-1}$ . Data are mean  $\pm$  s.d.,  $n = 3$  independent experiments. Two-tailed unpaired  $t$ -tests. Raw data for the gels can be found in Supplementary Fig. 1i. \*\* $P < 0.01$ , \*\*\* $P < 0.001$ , \*\*\*\* $P < 0.0001$ .

signals for 14 bp of dsDNA in the downstream DNA channel, 6 bp of upstream dsDNA located between the  $\beta'$  clamp helices and  $\beta$  protrusion, and a partially rewound transcription bubble (from upstream) with 5 nt of ntDNA remaining single-stranded (Fig. 3c,d, Extended Data Fig. 6h and Supplementary Video 4). The cryo-EM map shows no signal in the RNA exit channel and weak disconnected signal in the active centre cleft that probably originates from the non-specific rebinding of released RNA<sup>29</sup> (Fig. 3d). The map features suggest that this is an intermediate state of DNA–RNA release, in which RNA is released from the RNA exit channel, the transcription bubble is disrupted, and the ntDNA and tDNA of the transcription bubble are partially rewound (Fig. 3e and Supplementary Video 4).

The upstream dsDNA of TTC release undergoes a marked conformation change compared with that of TTC hairpin. The helix axis of the upstream dsDNA of TTC release rotates around 75° in an upward direction compared with that of TTC hairpin (Extended Data Fig. 7a). The rotation of the dsDNA relocates the 6-bp upstream dsDNA (–17 to –12) away from RNAP and thus becomes disordered in the structure (Extended Data Fig. 7b). The rewound 5-bp dsDNA (–10 to –6) were loosely restrained by the  $\beta$  protrusion, the  $\beta'$  coiled-coil and the  $\beta'$  rudder (Fig. 3f). Further rewinding of the upstream dsDNA is stopped by the  $\beta$  lobe domain and requires cleft opening to a greater extent (Fig. 3f). The 5-nt single-stranded ntDNA remains in the same location as in TTC pause and TTC hairpin (Fig. 3e). The 14-bp dsDNA of TTC release locates at the downstream dsDNA channel and makes interactions with RNAP as it does in an elongation complex (Extended Data Fig. 7c). Structural comparison shows that the RNAP clamp and lobe adopt the closed conformation seen in canonical elongation complex (Extended Data Fig. 7d), consistent with the previous findings that clamp opening is required for DNA release<sup>30</sup>. In short, our TTC-release structure suggests that DNA duplex remains bound to RNAP in a partially rewound form after RNA release.

The TTC-release complex also shows that transcription bubble rewinding is accompanied by hairpin completion and release of the nascent RNA<sup>31,32</sup>. The structure of the TTC-hairpin complex reveals that the –10 nucleotide of tDNA is ready to unpair with RNA and to rewind with the –10 nucleotide of ntDNA (Fig. 2j,k and Extended Data Fig. 5c–e). These results lead us to hypothesize that the rewinding of the transcription bubble triggers the subsequent steps of hairpin completion and RNA release. To test this model, we measured the termination efficiency at  $\lambda_{\text{IR}2}$  with pre-melted regions at various positions close to the termination site (Fig. 3g and Extended Data Fig. 8a). The results show that pre-melting the downstream half of the transcription bubble (D5, –5 to –1) has no effect on the termination at all, but pre-melting the upstream half of the transcription bubble (U5, –10 to –6) completely abolished termination (Fig. 3g). This result supports the ideas that rewinding of transcription bubble is required for intrinsic termination and that the process initiates from the upstream end, consistent with a previous report<sup>32</sup>. We next performed a more refined mapping to define the minimal requirements of bubble rewinding for efficient termination. Pre-melting two base pairs in the middle of the transcription bubble (–7/–6) had little effect. Moving the 2-bp pre-melted region upstream gradually decreased the termination efficiency. Of note, pre-melting the first two base pairs (–10/–9) completely abolished termination, highlighting the crucial role of rewinding the first two base pairs (–10/–9) during intrinsic termination (Fig. 3g). The same results were obtained using the  $\phi_{\text{T}500}$  terminator sequence (Extended Data Fig. 8b). These results support our hypothesis that rewinding the transcription bubble is an important step for intrinsic termination, which probably occurs by reducing the energetic barriers for hairpin completion and RNA release. We also noted that termination occurred, albeit with low efficiency, in response to asRNAs (asRNA –11 and –10) that form a duplex only in the RNA exit channel and do not disrupt the RNA–DNA hybrid<sup>33</sup> (Extended Data Fig. 8c). This result suggests that rewinding the transcription bubble is sufficient to induce termination

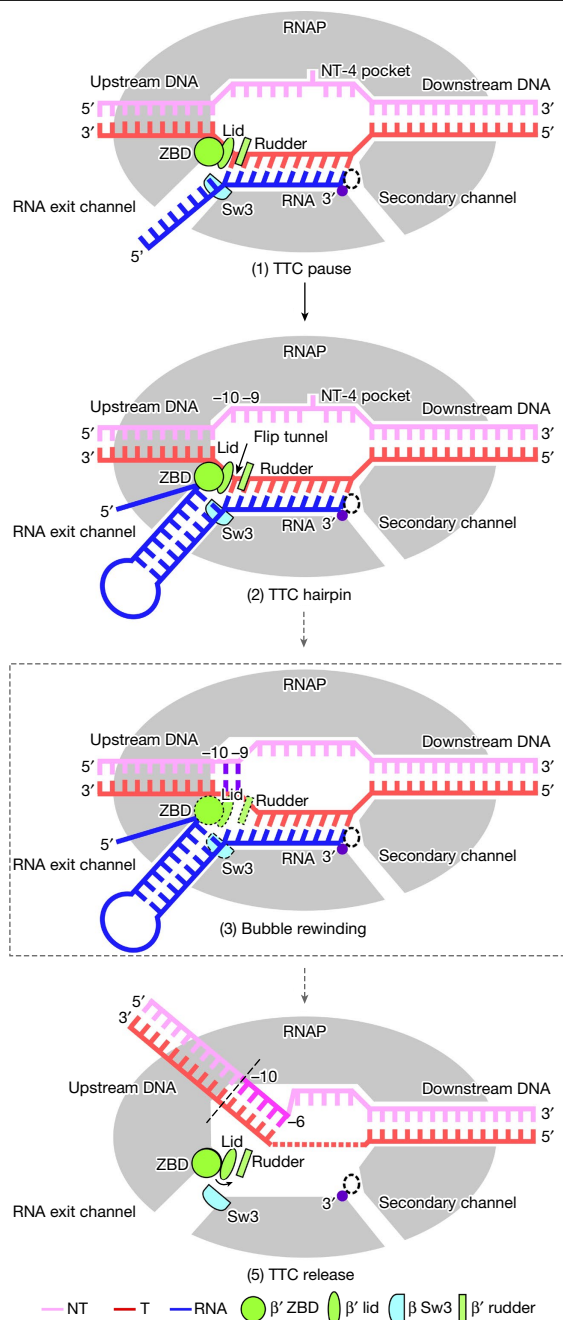


**Fig. 4 | The proposed pathway of intrinsic termination.** TTC-pause, TTC-hairpin and TTC-release structures were obtained in this study. Bubble rewinding is a proposed intermediate state in the pathway. See also Extended Data Fig. 9.

even without hairpin extension, consistent with bubble rewinding beginning the RNA release process. Together, our cryo-EM structures and in vitro transcription results suggest that rewinding the upstream two base pairs of the transcription bubble is a requisite for subsequent RNA hairpin completion and RNA release.

An intriguing implication of our structures is that the nascent RNA dissociates before RNAP releases dsDNA, consistent with evidence that terminated RNAP can remain associated with and slide on DNA after termination<sup>34,35</sup>. We tested this idea by measuring the rates of RNA and DNA release from TTC in physiologically relevant solutes using a scaffold that provided all RNAP–DNA contacts (Fig. 3h). After addition of asRNA to trigger termination, RNA was released approximately five

times more quickly than DNA. This result indicates that the binary RNAP–DNA complex survives after RNA release at the post-termination stage. This binary complex may dissociate more slowly in vivo where sliding RNAP would not immediately encounter a DNA end.

## Discussion

On the basis of our cryo-EM structures and biochemical evidence, we propose a detailed model for bacterial intrinsic termination (Fig. 4 and Extended Data Fig. 9): (1) RNAP pauses at the terminator site containing an elemental pause-like sequence motif<sup>4,12</sup> ( $S_{-10}U_{-1}$ ), where it adopts the ‘half-swivelled’ conformation that accommodates a half-translocated RNA–DNA hybrid in the active site cleft; (2) initial folding of terminator hairpin enlarges the RNA exit channel<sup>12,21</sup>, induces a ‘full-swivel’ RNAP conformation<sup>13,14,19</sup>, and weakens the upstream RNA–DNA base-pair interactions; (3) RNAP rewinds the two base pairs of the upstream transcription bubble and clears the energetic barrier for subsequent RNA hairpin completion<sup>31,32</sup>; (4) the terminator hairpin completes formation in the RNA exit channel by extracting the RNA out the exit channel either by ‘hybrid shearing’<sup>26</sup> (the RNA moves but tDNA does not), by pulling the RNA–DNA hybrid upstream by ‘forward translocation’<sup>26,27</sup> (the downstream duplex melts without nucleotide addition to RNA), or by extending the hairpin stem into the active site cleft by ‘hairpin invasion’<sup>12,25,28,36</sup> (the RNAP clamp opens to allow hairpin extension)—rewinding of the transcription bubble propagates concurrently with RNA hairpin completion; and (5) RNAP releases the nascent RNA but retains the partially rewound DNA<sup>34–36</sup>. RNAP may either slide on genomic DNA or finally dissociate DNA spontaneously or aided by pro-termination factors<sup>7,34,35,37–39</sup>.

In summary, our cryo-EM structures of transcription termination complexes reveal how bacterial RNAP pauses at intrinsic terminator sequences, how a terminator hairpin nucleates its folding in the RNA exit channel to weaken the RNA–DNA hybrid, how RNAP rewinds the transcription bubble to allow completion of the terminator hairpin and release of nascent RNA, and how RNAP retains the partially rewound dsDNA. The structures provide structural mechanisms for bacterial intrinsic termination. This mechanism of DNA rewinding-triggered RNA release provides clues for factor-independent termination at hairpin-less terminator sequences by eukaryotic RNAPIII<sup>40,41</sup>.

## Online content

Any methods, additional references, Nature Portfolio reporting summaries, source data, extended data, supplementary information, acknowledgements, peer review information; details of author contributions and competing interests; and statements of data and code availability are available at <https://doi.org/10.1038/s41586-022-05604-1>.

1. Ray-Soni, A., Bellecourt, M. J. & Landick, R. Mechanisms of bacterial transcription termination: all good things must end. *Annu. Rev. Biochem.* **85**, 319–347 (2016).
2. Proudfoot, N. J. Transcriptional termination in mammals: stopping the RNA polymerase II juggernaut. *Science* **352**, aad9926 (2016).
3. Arimbasseri, A. G. & Maraia, R. J. Mechanism of transcription termination by rna polymerase III utilizes a non-template strand sequence-specific signal element. *Mol. Cell* **58**, 1124–1132 (2015).
4. Yarnell, W. S. & Roberts, J. W. Mechanism of intrinsic transcription termination and antitermination. *Science* **284**, 611–615 (1999).
5. Vannini, A. & Cramer, P. Conservation between the RNA polymerase I, II, and III transcription initiation machineries. *Mol. Cell* **45**, 439–446 (2012).
6. Porrua, O. & Libri, D. Transcription termination and the control of the transcriptome: why, where and how to stop. *Nat. Rev. Mol. Cell Biol.* **16**, 190–202 (2015).
7. Roberts, J. W. Mechanisms of bacterial transcription termination. *J. Mol. Biol.* **431**, 4030–4039 (2019).
8. Nielsen, S., Yuzenkova, Y. & Zenkin, N. Mechanism of eukaryotic RNA polymerase III transcription termination. *Science* **340**, 1577–1580 (2013).

9. Mairhofer, J., Wittwer, A., Cserjan-Puschmann, M. & Striedner, G. Preventing T7 RNA polymerase read-through transcription-A synthetic termination signal capable of improving bioprocess stability. *ACS Synth. Biol.* **4**, 265–273 (2015).
10. Peters, J. M., Vangeloff, A. D. & Landick, R. Bacterial transcription terminators: the RNA 3'-end chronicles. *J. Mol. Biol.* **412**, 793–813 (2011).
11. Chen, Y. J. et al. Characterization of 582 natural and synthetic terminators and quantification of their design constraints. *Nat. Methods* **10**, 659–664 (2013).
12. Gusarov, I. & Nudler, E. The mechanism of intrinsic transcription termination. *Mol. Cell* **3**, 495–504 (1999).
13. Kang, J. Y. et al. RNA polymerase accommodates a pause RNA hairpin by global conformational rearrangements that prolong pausing. *Mol. Cell* **69**, 802–815.e801 (2018).
14. Guo, X. et al. Structural basis for NusA stabilized transcriptional pausing. *Mol. Cell* **69**, 816–827.e814 (2018).
15. Vos, S. M., Farnung, L., Urlaub, H. & Cramer, P. Structure of paused transcription complex Pol II–DSIF–NELF. *Nature* **560**, 601–606 (2018).
16. Kang, J. Y. et al. Structural basis of transcription arrest by coliphage HK022 Nun in an *Escherichia coli* RNA polymerase elongation complex. *eLife* **6**, e25478 (2017).
17. Vvedenskaya, I. O. et al. Interactions between RNA polymerase and the ‘core recognition element’ counteract pausing. *Science* **344**, 1285–1289 (2014).
18. Larson, M. H. et al. A pause sequence enriched at translation start sites drives transcription dynamics in vivo. *Science* **344**, 1042–1047 (2014).
19. Zhu, C. et al. Transcription factors modulate RNA polymerase conformational equilibrium. *Nat. Commun.* **13**, 1546 (2022).
20. Yang, Y. et al. Structural visualization of transcription activated by a multidrug-sensing MerR family regulator. *Nat. Commun.* **12**, 2702 (2021).
21. Lubkowska, L., Maharjan, A. S. & Komissarova, N. RNA folding in transcription elongation complex: implication for transcription termination. *J. Biol. Chem.* **286**, 31576–31585 (2011).
22. King, R. A., Markov, D., Sen, R., Severinov, K. & Weisberg, R. A. A conserved zinc binding domain in the largest subunit of DNA-dependent RNA polymerase modulates intrinsic transcription termination and antitermination but does not stabilize the elongation complex. *J. Mol. Biol.* **342**, 1143–1154 (2004).
23. Touloukhanov, I. & Landick, R. The flap domain is required for pause RNA hairpin inhibition of catalysis by RNA polymerase and can modulate intrinsic termination. *Mol. Cell* **12**, 1125–1136 (2003).
24. Ray-Soni, A., Mooney, R. A. & Landick, R. Trigger loop dynamics can explain stimulation of intrinsic termination by bacterial RNA polymerase without terminator hairpin contact. *Proc. Natl Acad. Sci. USA* **114**, E9233–E9242 (2017).
25. Komissarova, N., Becker, J., Solter, S., Kireeva, M. & Kashlev, M. Shortening of RNA:DNA hybrid in the elongation complex of RNA polymerase is a prerequisite for transcription termination. *Mol. Cell* **10**, 1151–1162 (2002).
26. Larson, M. H., Greenleaf, W. J., Landick, R. & Block, S. M. Applied force reveals mechanistic and energetic details of transcription termination. *Cell* **132**, 971–982 (2008).
27. Santangelo, T. J. & Roberts, J. W. Forward translocation is the natural pathway of RNA release at an intrinsic terminator. *Mol. Cell* **14**, 117–126 (2004).
28. Epshtein, V., Cardinale, C. J., Ruckenstein, A. E., Borukhov, S. & Nudler, E. An allosteric path to transcription termination. *Mol. Cell* **28**, 991–1001 (2007).
29. Kashlev, M. & Komissarova, N. Transcription termination: primary intermediates and secondary adducts. *J. Biol. Chem.* **277**, 14501–14508 (2002).
30. Bellecourt, M. J., Ray-Soni, A., Harwig, A., Mooney, R. A. & Landick, R. RNA polymerase clamp movement aids dissociation from DNA but is not required for RNA release at intrinsic terminators. *J. Mol. Biol.* **431**, 696–713 (2019).
31. Park, J. S. & Roberts, J. W. Role of DNA bubble rewinding in enzymatic transcription termination. *Proc. Natl Acad. Sci. USA* **103**, 4870–4875 (2006).
32. Ryder, A. M. & Roberts, J. W. Role of the non-template strand of the elongation bubble in intrinsic transcription termination. *J. Mol. Biol.* **334**, 205–213 (2003).
33. Shankar, S., Hatoum, A. & Roberts, J. W. A transcription antiterminator constructs a NusA-dependent shield to the emerging transcript. *Mol. Cell* **27**, 914–927 (2007).
34. Harden, T. T. et al. Alternative transcription cycle for bacterial RNA polymerase. *Nat. Commun.* **11**, 448 (2020).
35. Kang, W. et al. Transcription reinitiation by recycling RNA polymerase that diffuses on DNA after releasing terminated RNA. *Nat. Commun.* **11**, 450 (2020).
36. Dey, S. et al. Structural insights into RNA-mediated transcription regulation in bacteria. *Mol. Cell* **82**, 3885–3900.e3810 (2022).
37. Pei, H. H. et al. The delta subunit and NTPase HelD institute a two-pronged mechanism for RNA polymerase recycling. *Nat. Commun.* **11**, 6418 (2020).
38. Kouba, T. et al. Mycobacterial HelD is a nucleic acids-clearing factor for RNA polymerase. *Nat. Commun.* **11**, 6419 (2020).
39. Newing, T. P. et al. Molecular basis for RNA polymerase-dependent transcription complex recycling by the helicase-like motor protein HelD. *Nat. Commun.* **11**, 6420 (2020).
40. Hou, H. et al. Structural insights into RNA polymerase III-mediated transcription termination through trapping poly-deoxythymidine. *Nat. Commun.* **12**, 6135 (2021).
41. Girbig, M. et al. Architecture of the yeast Pol III pre-termination complex and pausing mechanism on poly(dT) termination signals. *Cell Rep.* **40**, 111316 (2022).

**Publisher’s note** Springer Nature remains neutral with regard to jurisdictional claims in published maps and institutional affiliations.

Springer Nature or its licensor (e.g. a society or other partner) holds exclusive rights to this article under a publishing agreement with the author(s) or other rightsholder(s); author self-archiving of the accepted manuscript version of this article is solely governed by the terms of such publishing agreement and applicable law.

© The Author(s), under exclusive licence to Springer Nature Limited 2023

## Methods

## Plasmid construction

Plasmid pET28a-TEV-*Ec*- $\sigma^{70}$  (Supplementary Table 1) was constructed by inserting the *E. coli*  $\sigma^{70}$  gene amplified using Phanta Max Super-Fidelity DNA Polymerase (Vazyme Biotech) from *E. coli* genomic DNA into a modified pET28a plasmid carrying the TEV protease cleavage site by a homogenous recombination method (pEASY-Basic Seamless Cloning and Assembly Kit, Transgen Biotech). Derivatives of pRL706 were constructed by primer-mediated, site-directed mutagenesis using NEB Q5 site-directed mutagenesis reagents.

*E. coli* RNAP core enzyme

The *E. coli* RNAP core enzyme for cryo-EM and most in vitro assays was over-expressed from *E. coli* BL21(DE3) (Novo protein) carrying p*Ec*ABC and pCDF-*Ec* rpoZ (Supplementary Table 1) and purified as described<sup>42</sup>. *E. coli* RNAP core enzyme used in experiments shown in Fig. 3h and Extended Data Fig. 8c was purified as described previously<sup>43</sup>.

*E. coli* RNAP core enzyme with substitutions in the  $\beta$  subunit used in experiments shown in Extended Data Fig. 3 was purified using  $\beta$ -subunit overexpression from pRL706 derivatives (Supplementary Table 1). Each plasmid was independently transformed into *E. coli* strain RL1204 (Supplementary Table 1) and a single colony was inoculated into 30 ml LB + 100  $\mu$ g ml<sup>-1</sup> carbenicillin and grown overnight at 37 °C. The saturated cell culture was added to 1 l fresh LB + 100  $\mu$ g ml<sup>-1</sup> carbenicillin and grown at 37 °C with adequate aeration by orbital shaking in a Fernbach flask until apparent  $A_{600}$  reached 0.2.  $\beta$  subunit overexpression was induced by adding IPTG (Gold Biotechnology) to 1 mM and cell growth was monitored until apparent  $A_{600}$  reached 0.9. The cells were collected and homogenized by sonication in 30 ml lysis buffer (50 mM Tris-HCl, pH 7.9, 5% v/v glycerol, 233 mM NaCl, 2 mM EDTA, 10 mM  $\beta$ -mercaptoethanol, 100  $\mu$ g ml<sup>-1</sup> PMSF, 1 tablet of protease inhibitor cocktail (Roche), and 10 mM DTT). After removing cell debris by centrifugation (27,000g, 15 min, 4 °C), DNA binding proteins including target RNAPs were precipitated by addition of polyethyleneimine (PEI, Sigma-Aldrich) to 0.6% (w/v) final and stirred for at least 10 min. After centrifugation (11,000g, 15 min, 4 °C), the protein pellet was resuspended in 25 ml PEI wash buffer (10 mM Tris-HCl, pH 7.9, 5% v/v glycerol, 0.1 mM EDTA, 5  $\mu$ M ZnCl<sub>2</sub>, 500 mM NaCl) to remove non-target proteins. After centrifugation (11,000g, 15 min, 4 °C), RNAP was eluted from the pellet into 25 ml PEI Elution Buffer (10 mM Tris-HCl, pH 7.9, 5% v/v glycerol, 0.1 mM EDTA, 5  $\mu$ M ZnCl<sub>2</sub>, 1 M NaCl). The crude extract of RNAP was subjected to sequential FPLC purifications using Ni<sup>2+</sup>-affinity (HisTrap FF 5 ml, Cytiva), followed by purification using a Heparin column (HiTrap FF 5 ml, Cytiva). The purified RNAPs were dialysed into RNAP Storage Buffer (10 mM Tris-HCl, 25% v/v glycerol, 100 mM NaCl, 100  $\mu$ M EDTA, 1 mM MgCl<sub>2</sub>, 20  $\mu$ M ZnCl<sub>2</sub>, 10 mM DTT). Samples were aliquoted, flash frozen in liquid nitrogen and stored in -80 °C.

*E. coli*  $\sigma^{70}$ 

*E. coli*  $\sigma^{70}$  (*Ec*- $\sigma^{70}$ ) was over-expressed in *E. coli* BL21(DE3) cells (Novo protein) carrying pET28a-TEV-*Ec*- $\sigma^{70}$  (Supplementary Table 1). Protein expression was induced with 0.3 mM IPTG at 18 °C for 14 h when  $A_{600}$  reached to 0.6–0.8. Cell pellet was lysed in lysis buffer B (50 mM Tris-HCl, pH 7.7, 500 mM NaCl, 5% (v/v) glycerol, 5 mM  $\beta$ -mercaptoethanol, and 0.1 mM PMSF) using an Avestin EmulsiFlex-C3 cell disrupter (Avestin). The lysate was centrifuged (16,000g; 50 min; 4 °C) and the supernatant was loaded on to a 2 ml column packed with Ni-NTA agarose beads (Smart-Lifesciences). The bound proteins were washed by lysis buffer B containing 20 mM imidazole and eluted with the lysis buffer B containing 400 mM imidazole. The eluted fractions were supplemented with TEV protease and transferred to a dialysis bag to exchange buffer to 20 mM Tris-HCl, pH 7.7, 150 mM NaCl, 5% (v/v) glycerol, 5 mM  $\beta$ -mercaptoethanol. The sample was reloaded

onto the Ni-NTA column, and the tag-free protein was retrieved from the flow-through fraction. The sample was diluted, loaded onto a Q HP column (HiPrep Q HP 16/10, Cytiva) and eluted with a salt gradient of buffer A (50 mM Tris-HCl, pH 7.7, 150 mM NaCl, 5% (v/v) glycerol, 1 mM DTT) and buffer B (50 mM Tris-HCl, pH 7.7, 500 mM NaCl, 5% (v/v) glycerol, 1 mM DTT). The fractions containing target proteins were collected, concentrated to 5.2 mg ml<sup>-1</sup>, and stored at -80 °C.

*E. coli*  $\sigma^{70}$  used in experiments shown in Extended Data Figs. 3 and 8c was purified as described previously<sup>43</sup>.

*E. coli* RNAP holoenzyme

*E. coli* RNAP core (3  $\mu$ M, final concentration) and  $\sigma^{70}$  (12  $\mu$ M, final concentration) were incubated in 0.5 ml 20 mM Tris-HCl, pH 7.7, 100 mM NaCl, 1% (v/v) glycerol, 1 mM DTT for 2 h at 4 °C. The reaction mixture was applied to a Superdex 200 10/300 column (Cytiva) equilibrated in 20 mM Tris-HCl, pH 7.7, 100 mM NaCl, 1% (v/v) glycerol, 1 mM DTT. Fractions containing RNAP holoenzyme were collected and concentrated to -5 mg ml<sup>-1</sup>, and stored at -80 °C.

## Nucleic acid scaffolds

Nucleic acid scaffolds (Supplementary Table 1) for cryo-EM study of *E. coli* TTC pause and TTC hairpin were prepared as follows: non-template strand DNA (5'-GGCGTACGGAAAATAACACGGCGAATACCC-3'; 0.3 mM, final concentration; Sangon Biotech), template strand DNA (5'-GGGTATTCGCCGTGAATAAAAAGGGTACGCC-3'; 0.33 mM, final concentration; Sangon Biotech) and RNA (5'-GCGUCCAGGCCUUUUUUUU-3'; 0.39 mM, final concentration; GenScript Biotech) in 50  $\mu$ l annealing buffer (5 mM Tris-HCl, pH 8.0, 200 mM NaCl, and 10 mM MgCl<sub>2</sub>) were heated for 5 min at 95 °C, cooled to 22 °C in 2 °C steps with 30 s per step using a thermal cycler.

Nucleic acid scaffold (Supplementary Table 1) for cryo-EM study of *E. coli* TTC release was prepared as follows: template strand DNA (5'-GGGTATTCGCCGTGAATAAAAAGGGTACGCC-3'; 0.39 mM, final concentration; Sangon Biotech) and RNA (5'-Cy5-ACGCGUCGAGGCCUUUUUUUU-3'; 0.3 mM, final concentration; GenScript Biotech Corp.) in 50  $\mu$ l annealing buffer (5 mM Tris-HCl, pH 8.0, 200 mM NaCl, and 10 mM MgCl<sub>2</sub>) were heated for 5 min at 95 °C and then cooled to 22 °C in 2 °C steps with 30 s per step using a thermal cycler.

For experiments shown in Fig. 3g and Extended Data Figs. 3 and 8c, DNA and RNA oligonucleotides (Extended Data Fig. 8c and Supplementary Table 1) were obtained from Integrated DNA Technologies (IDT) and were purified by denaturing polyacrylamide gel electrophoresis (PAGE; 15% 19:1 acrylamide: bis-acrylamide, 45 mM Tris-borate, pH 8.3, 1.25 mM Na<sub>2</sub>EDTA, 8 M urea) before use, unless otherwise stated. [ $\gamma$ -<sup>32</sup>P] ATP, [ $\alpha$ -<sup>32</sup>P]UTP and [ $\alpha$ -<sup>32</sup>P]GTP were obtained from PerkinElmer Life Sciences; rNTPs were obtained from Promega; and 3'-deoxy GTP (3'dGTP) was obtained from Jena Bioscience.

## Cryo-EM data collection and processing

*E. coli* TTC pause. *E. coli* RNAP core enzyme (20  $\mu$ M, final concentration) and the nucleic acid scaffold (26  $\mu$ M, final concentration) were incubated in 0.5 ml 10 mM HEPES, pH 7.5, 5 mM KCl, 5 mM MgCl<sub>2</sub>, 3 mM DTT at room temperature for 50 min. The mixture was applied to a Superdex 200 10/300 column (Cytiva) equilibrated in 10 mM HEPES, pH 7.5, 5 mM KCl, 5 mM MgCl<sub>2</sub>, 3 mM DTT. Fractions containing TTC-pause complex were collected and concentrated to 13 mg ml<sup>-1</sup>.

The freshly purified *E. coli* TTC pause at 13 mg ml<sup>-1</sup> was incubated with 3-([3-cholamidopropyl] dimethylammonio)-2-hydroxy-1-propanesulfonate (CHAPSO, 8 mM, final concentration; Hampton Research) prior to grid preparation. The complex (3  $\mu$ l) was subsequently applied on a glow-discharged C-flat CF-1.2/1.3-4Cu-T-50 400 mesh holey carbon grids (Electron Microscopy Sciences), blotted with Vitrobot Mark IV (FEI), and plunge-frozen in liquid ethane with 95% chamber humidity at 10 °C.



The data were collected on a 300 keV Titan Krios (FEI) equipped with a K2 Summit direct electron detector (Gatan) at National Center for Protein Sciences Shanghai. A total of 1,796 images were recorded using Serial EM<sup>44</sup> in super-resolution counting mode with a pixel size of 1.0 Å, and a dose rate of 8 electrons per pixel per s. Movies were recorded at 200 ms per frame for 7.6 s (38 frames total) and defocus range was varied between -1.2 μm and -2.2 μm. Frames of individual movies were aligned using MotionCor2<sup>45</sup>, and contrast transfer function (CTF) estimations were performed using CTFFIND4<sup>46</sup>. About 1,000 particles were picked and subjected to 2D classification in RELION 3.0<sup>47</sup>. The resulting distinct 2D classes were used as templates and a total of 497,373 particles were picked out. The resulting particles were subjected to 2D classification in RELION 3.0 by specifying 100 classes<sup>47</sup>. Poorly populated classes were removed. We used a 50 Å low-pass-filtered map calculated from the structure of *E. coli* RNAP core enzyme (PDB: 6ALF) as the starting reference model for 3D classification ( $n = 3$ ). The final concentration maps calculated from 132,648 particles were obtained through 3D auto-refinement, CTF refinement, Bayesian polishing, and postprocessing in RELION 3.0. Gold standard Fourier shell correlation analysis indicated a mean map resolution of 3.58 Å (Extended Data Fig. 1)

The model of the RNAP core enzyme from the cryo-EM structure of *E. coli* TEC (PDB: 6ALF) was manually fit into the cryo-EM density map using Chimera<sup>48</sup>. Rigid-body and real-space refinement was performed in Coot<sup>49</sup> and Phenix<sup>50</sup>.

***E. coli* TTC hairpin.** The freshly purified *E. coli* TTC-pause complex (13 mg ml<sup>-1</sup>, 33 μM, final concentration) and asRNA (asRNA10, 330 μM, final concentration) were incubated in 30 μl 10 mM HEPES, pH 7.5, 5 mM KCl, 5 mM MgCl<sub>2</sub>, 3 mM DTT for 3 h at 4 °C. The sample was vitrified by the same procedure as for the TTC-pause complex.

The data were collected on a 300 keV Titan Krios (FEI) equipped with a K2 Summit direct electron detector (Gatan) at the Center of Electron Microscopy, Zhejiang University. A total of 3,888 images were recorded using Serial EM<sup>44</sup> in counting mode with a pixel size of 1.307 Å, and a dose rate of 9.9 electrons per pixel per s. Movies were recorded at 250 ms per frame for 10 s (40 frames total) and defocus range was varied between -1.8 μm and -2.6 μm. Frames of individual movies were aligned using MotionCor2<sup>45</sup>, and CTF estimations were performed using CTFFIND4<sup>46</sup>. About 1,548 particles were picked and subjected to 2D classification in RELION 3.0<sup>47</sup>. The resulting distinct 2D classes were used as templates and a total of 497,373 particles were picked out. The resulting particles were subjected to 2D classification in RELION 3.0 by specifying 100 classes<sup>47</sup>. Poorly populated classes were removed. We used a 50 Å low-pass-filtered map calculated from structure of *E. coli* RNAP core enzyme<sup>16</sup> (PDB: 6ALF) as the starting reference model for 3D classification ( $n = 4$ ). Two same classes were combined and 360,313 particles were used for 3D auto-refinement. To resolve heterogeneity around RNA hairpin in RNA exit channel, a soft mask that excludes RNA duplex and nearby protein regions (β' ZBD, β' dock, β flap, β CTR) was generated in Chimera and RELION 3.0. The mask was used to make a subtracted particle stack in RELION 3.0. The subtracted particles were applied for masked 3D classification ( $n = 6$ , without alignment), the best-resolved class containing obvious RNA hairpin (293,294 particles) was used for 3D auto-refinement, CTF refinement and Bayesian polishing and postprocessing. Gold standard Fourier shell correlation analysis indicated a mean map resolution of 3.05 Å (Extended Data Fig. 4). The structural model of RNAP core enzyme from the cryo-EM structure of *E. coli* hisPEC (PDB: 6ASX) was manually fit into the cryo-EM density map using Chimera<sup>48</sup>. Rigid-body and real-space refinement was performed in Coot<sup>49</sup> and Phenix<sup>50</sup>.

***E. coli* TTC release.** *E. coli* RNAP core enzyme (20 μM, final concentration) and nucleic acid scaffold comprising tDNA and RNA (30 μM, final concentration) were incubated in 0.5 ml 10 mM HEPES, pH 7.5,

50 mM KCl, 5 mM MgCl<sub>2</sub>, 3 mM DTT at room temperature for 30 min. The ntDNA (200 μM, final concentration) was subsequently added and the mixture was further incubated at room temperature for 30 min. The mixture was applied to a Superdex 200 10/300 column (Cytiva) equilibrated in 10 mM HEPES, pH 7.5, 50 mM KCl, 5 mM MgCl<sub>2</sub>, 3 mM DTT. Fractions containing TTC-pause complex were collected and concentrated to 17 mg ml<sup>-1</sup> (-43 μM), then the sample mixed with CHAPSO (Hampton Research) to a final concentration 8 mM, 430 μM (final concentration) asRNA12 was added and the reaction was incubated for 3 min prior to grid preparation. The complex (3 μl) was quickly applied on a glow-discharged UltraAuFoil R1.2/1.3 300 mesh holey Au grids (Quantifoil Micro Tools GmbH), blotted with Vitrobot Mark IV (FEI), and plunge-frozen in liquid ethane with 100% chamber humidity at 22 °C.

The data were collected on a 300 keV Titan Krios (FEI) equipped with a K3 Summit direct electron detector (Gatan) at National Center for Protein Sciences Shanghai. A total of 1,355 images were recorded using the EPU using super-resolution counting mode for 2.67 s exposures in 40 frames to give a total dose of 49.65 electrons per Å<sup>2</sup> with defocus range of -1.2 to -2.2 μm. Frames of individual movies were aligned using MotionCor2<sup>45</sup>, and contrast transfer-function estimations were performed using CTFFIND4<sup>46</sup>. About 1,000 particles were picked and subjected to 2D classification in RELION 3.0<sup>47</sup>. The resulting distinct 2D classes were served as templates for auto-picking and a total of 592,713 particles were picked out. The resulting particles were subjected to 2D classification in RELION 3.0 by specifying 100 classes<sup>47</sup>. Poorly populated classes were removed. We used a 50-Å low-pass-filtered map calculated from the TTC-hairpin map as the starting reference model for 3D classification ( $n = 6$ ). Two classes were combined and 282,423 the particle numbers used for 3D auto-refinement. To resolve heterogeneity about the DNA and RNA in the main cleft, a soft map that excludes the upstream dsDNA, the transcription bubble, the RNA-DNA hybrid, the downstream dsDNA, and the β' clamp domain nearby was generated in Chimera and RELION 3.0. The mask was used to make a subtracted particle stack in RELION 3.0. The subtracted particles were applied for masked 3D classification ( $n = 6$ , without alignment), the 3D class of TTC release (54,309 particles) were used for 3D auto-refinement, CTF refinement and Bayesian polishing and postprocessing. Gold standard Fourier shell correlation analysis indicated a mean map resolution of 3.48 Å (map A in Extended Data Fig. 6d). The structural model of RNAP core enzyme from the cryo-EM structure of *E. coli* hisPEC (PDB: 6ASX) was manually fit into the cryo-EM map using Chimera<sup>48</sup>. Rigid-body and real-space refinement was performed in Coot<sup>49</sup> and Phenix<sup>50</sup>. The other two major classes were also processed under the similar procedure resulting in two maps at 3.40 Å (map B and C in Extended Data Fig. 6d), both of which show little signal for the upstream dsDNA, the non-template ssDNA, and the ssRNA in the RNA exit channel, although clear signals for the downstream dsDNA and the half-translocated RNA-DNA hybrid. These features suggest that these two complexes were probably not properly assembled during complex reconstitution.

### Fluorescence-detected RNA release assay

To study asRNA-induced RNA release, *E. coli* RNAP core enzyme (200 nM, final concentration) and TTC-release nucleic acid scaffold (800 nM, final concentration) comprising Cy5-labelled RNA and tDNA were incubated in 300 μl transcription buffer (50 mM Tris-HCl, pH 8.0, 50 mM KCl, 5 mM MgCl<sub>2</sub>, 5 mM β-mercaptoethanol) at room temperature for 15 min. Then ntDNA (2 μM, final concentration) was subsequently added and the mixture was further incubated at room temperature for 15 min to form TTC-pause complex. The complex was immobilized on 150 μl Ni-NTA agarose beads (Smart-Lifesciences) pre-washed with transcription buffer. The immobilized complex was washed with 300 μl transcription buffer for three times. The reaction mixture was aliquoted and each of the aliquot (70 μl) was supplemented with 7 μl asRNA12 (final concentration: 1 μM) to induce RNA release. For each of the aliquots, 20 μl reaction mixtures were taken out as reference of total

amount of nascent RNA. The resulting reaction mixtures (50  $\mu$ l) were separated into supernatant and pellet fractions by centrifugation at specified time points. Both the total and supernatant samples (20  $\mu$ l) were mixed with 5  $\mu$ l loading buffer (8 M urea, 20 mM EDTA, 0.025% xylene cyanol), 95 °C boiled for 5 min, and cooled down in ice for 5 min. RNA were separated by 20% urea-polyacrylamide slab gels (19:1 acrylamide:bis-acrylamide) in 90 mM Tris-borate, pH 8.0 and 0.2 mM EDTA and analysed by fluorescein scanning (Typhoon; GE Healthcare).

### Release assay to measure RNA and DNA rates release during intrinsic termination

The TTC-release scaffold (Fig. 3a) was modified by addition of 12 downstream base pairs to eliminate any effect of RNAP–DNA-end contacts that could affect the DNA release rate (Fig. 3h). Elongation complexes were reconstituted one nucleotide upstream from the U8 termination site by incubation of 1  $\mu$ M RNA21, 200 nM tDNA that was 5' <sup>32</sup>P-labelled by treatment with [ $\gamma$ -<sup>32</sup>P]ATP polynucleotide kinase, and 400 nM *E. coli* core RNAP in 100  $\mu$ l EC buffer (10 mM Hepes, pH 8.0, 50 mM potassium glutamate, 10 mM magnesium acetate, 0.1 mM EDTA, 5  $\mu$ g acetylated BSA per ml and 1 mM DTT) for 5 min at 37 °C. Non-template DNA (2  $\mu$ M) was added and the mixture was incubated for an additional 5 min at 37 °C. The final ratio of RNAP:RNA:template DNA:non-template DNA was 2.5:1:10. The estimated concentration of the assembled transcription termination complex was 200 nM. Heparin (50  $\mu$ g ml<sup>-1</sup>) was added to the mixture to prevent core RNAP from rebinding to the scaffold after release. The RNA was extended to U8 by reaction with 2  $\mu$ M [ $\alpha$ -<sup>32</sup>P]UTP (136 Ci mmol<sup>-1</sup>) yielding TTC with 5' <sup>32</sup>P-labelled T DNA and 3' <sup>32</sup>P-labelled RNA. The complex was immobilized on 20  $\mu$ l of Ni-NTA agarose beads (Qiagen) with occasional pipetting. After 10 min incubation at room temperature, the immobilized complex was washed with EC buffer (5 cycles of centrifugation and resuspension of the pelleted beads in 200  $\mu$ l of fresh EC buffer). The washed bead complex was resuspended in 200  $\mu$ l EC buffer. One 5- $\mu$ l portion was mixed with 5  $\mu$ l stop buffer (8 M urea, 50 mM EDTA, 90 mM Tris-Borate buffer, pH 8.3, 0.02% bromophenol blue, 0.02% xylene cyanol) for total zero-timepoint sample. A second 5  $\mu$ l portion was incubated with ATP, CTP, and 3'-dGTP (150  $\mu$ M each), then combined with stop buffer as a check for TTC integrity. (Fig. 3h). The magnetic Ni-NTA beads were pulled to one side using a magnet, then 25  $\mu$ l of the supernatant was passed through a nitrocellulose microfilter plate (384 wells) placed on top of a multi-well plate vacuum manifold (Operated at 20 Hg) with a receiver plate on the bottom (Pall Corporation). A portion (5  $\mu$ l) of the filtrate was mixed with 5  $\mu$ l stop buffer for the released 0-timepoint sample. To initiate the termination reaction and monitor RNA and DNA release, asRNA12 (Fig. 3h) was added to a final concentration of 1  $\mu$ M and supernatant (25  $\mu$ l) was removed after 10, 20, 30, 60, 120 and 180 s, filtered, and combined with stop buffer as described for the zero-timepoint sample. Samples were then analysed by denaturing PAGE (15% 19:1 acrylamide: bis-acrylamide, 45 mM Tris-borate, pH 8.3, 1.25 mM Na<sub>2</sub>EDTA, 8 M urea) for 2 h at 60 W, the gel was exposed on a Storage Phosphor Screen and imaged on a Typhoon PhosphorImager (GE Healthcare). The RNA and T DNA were quantified using ImageJ software (NIH). Released RNA and DNA were compared with the total samples to calculate fractions remaining in the TTC from triplicate reactions. The changes in the fractions over time were fit to a first-order dissociation rate equation with a small fraction that remained bound to the beads (recalcitrant to release) (Fig. 3h). The recalcitrant fractions (both RNA and DNA) were 0.05 for the first replicate and 0.13 for the second and third replicates. One timepoint (30 s) was lost for replicate 1.

### In vitro transcription assay

DNA templates used for in vitro transcription assays contains the T5-N25 promoter, a coding region, and the  $\lambda$ <sub>R2</sub> terminator. The DNA template was prepared by PCR primer extension using the single-stranded ntDNA (5'-TCATAAAAAATTTATTTGCTTTCAGGAAAATTTTTC

TGTATAATAGATTCATAAATTTGAGAGAGGAGTTTAAATCCAGGCCTGCTGGTAATCCAGGCCTTTTATTTGGATCCCCGGGTAGAATTCG-3'; 1  $\mu$ M; RuiMian) as template and tDNA (5'-CGAATTCTACCCGGGATCCAAATAAAAAGGCCTGCGATTACCAGCAGGCCTGGATTTATGATCCCGGAGGAGAAGCAGAGGTACC-3'; 2  $\mu$ M; Sangon Biotech) as the primer in a thermal cycler. The efficiency of primer extension was confirmed on a 1.5% agarose gel and the extended dsDNA were further purified by a Gel Extraction Kit (Omega Bio-Tek). The pre-melted DNA templates were prepared by the same procedure using tDNA primer with non-complementary sequences at the specified positions (Fig. 3g and Extended Data Fig. 8a,b).

Reaction mixture (20  $\mu$ l) in transcription buffer (40 mM Tris-HCl, pH 8.0, 75 mM NaCl, 5 mM MgCl<sub>2</sub>, 12.5% glycerol, 2.5 mM DTT, and 50  $\mu$ g ml<sup>-1</sup> BSA) containing RNAP holoenzyme (50 nM) and DNA template (50 nM) were incubated for 10 min at 37 °C. RNA synthesis was initiated by addition of 1.2  $\mu$ l NTP mixture (5  $\mu$ M ATP, 5  $\mu$ M GTP, 0.05  $\mu$ M UTP and 0.03  $\mu$ M [ $\alpha$ -<sup>32</sup>P]UTP (45 Bq fmol<sup>-1</sup>), final concentration) for 10 min at 37 °C to obtain TECs halted at U25. Subsequently, 1  $\mu$ l heparin (50  $\mu$ g ml<sup>-1</sup>; final concentration) was added to only allow a single round of transcription. RNA extension was resumed by addition of 1  $\mu$ l NTP mixture (5  $\mu$ M ATP, 5  $\mu$ M CTP, 5  $\mu$ M GTP, and 5  $\mu$ M UTP; final concentration). Reactions were terminated by adding 5  $\mu$ l loading buffer, boiled at 95 °C for 5 min, and cooled in ice for 5 min. The RNA transcripts were separated by 12% urea-polyacrylamide slab gels (19:1 acrylamide:bis-acrylamide) in 90 mM Tris-borate, pH 8.0 and 0.2 mM EDTA and analysed by Storage Phosphor scanning (Typhoon; GE Healthcare).

Promoter-based template DNA sequences with a  $\lambda$ P<sub>R</sub> promoter, C-less cassette, and wild-type or variant  $\lambda$ t<sub>R2</sub> or  $\phi$ 82t<sub>500</sub> terminators for experiments shown in Extended Data Figs. 3 and 8c were PCR-amplified using primers flanking both ends and gel-purified using Qiagen Qiaquick purification reagents. NusA protein was purified as described previously<sup>51</sup>. Core RNAP was incubated with  $\sigma$ <sup>70</sup> for 30 min at 37 °C to form holo-RNAP. To initiate transcription, holo-RNAP (31.25 nM) was incubated with template DNA (25 nM), ApU (150  $\mu$ M), ATP + UTP (both at 2.5  $\mu$ M), and 2  $\mu$ M [ $\alpha$ -<sup>32</sup>P]GTP (54.5 Ci mmol<sup>-1</sup>) in EC buffer for 5 min at 37 °C to form a halted complex at A26. Transcription was then restarted by adding a master mix containing NTP mix (A+C+G+U), heparin and potassium glutamate at a final concentration of 150  $\mu$ M, 50  $\mu$ g ml<sup>-1</sup> and 100 mM respectively. Reactions were stopped and products were separated as described above. The termination efficiencies were calculated from three independent replicates.

For experiments shown in Extended Data Fig. 3f, elongation complexes were reconstituted 15 nucleotides upstream from the U8 termination site by incubation of 25 nM RNA23, 50 nM T DNA, and 50 nM *E. coli* core RNAP in 50  $\mu$ l EC buffer for 5 min at 37 °C. Non-template DNA (125 nM) was added and the mixture was incubated for an additional 5 min at 37 °C. Heparin (50  $\mu$ g ml<sup>-1</sup>) was added to the mixture to prevent core RNAP from rebinding to nucleic acids. The RNA was extended to A25 by a reaction with ATP + CTP (2.5  $\mu$ M final for both) followed by radiolabelling to G27 by reacting with 0.037  $\mu$ M [ $\alpha$ -<sup>32</sup>P]GTP (3,000 Ci mmol<sup>-1</sup>). The RNA was then extended to the termination site by addition of 100  $\mu$ M NTP mix.

### Reporting summary

Further information on research design is available in the Nature Portfolio Reporting Summary linked to this article.

### Data availability

The cryo-EM map and coordinates have deposited in Protein Data Bank with accession numbers 7YP9 (TTC pause), 7YPA (TTC hairpin) and 7YPB (TTC release) and in the Electron Microscopy Data Bank under accession numbers EMD-33996 (TTC pause), EMD-33997 (TTC hairpin) and EMD-33998 (TTC release). Source data are provided with this paper.

42. Hudson, B. P. et al. Three-dimensional EM structure of an intact activator-dependent transcription initiation complex. *Proc. Natl Acad. Sci. USA* **106**, 19830–19835 (2009).
43. Hein, P. P. et al. RNA polymerase pausing and nascent-RNA structure formation are linked through clamp-domain movement. *Nat. Struct. Mol. Biol.* **21**, 794–802 (2014).
44. Mastronarde, D. N. Automated electron microscope tomography using robust prediction of specimen movements. *J. Struct. Biol.* **152**, 36–51 (2005).
45. Zheng, S. Q. et al. MotionCor2: anisotropic correction of beam-induced motion for improved cryo-electron microscopy. *Nat. Methods* **14**, 331–332 (2017).
46. Rohou, A. & Grigorieff, N. CTFFIND4: Fast and accurate defocus estimation from electron micrographs. *J. Struct. Biol.* **192**, 216–221 (2015).
47. Zivanov, J. et al. New tools for automated high-resolution cryo-EM structure determination in RELION-3. *eLife* **7**, e42166 (2018).
48. Pettersen, E. F. et al. UCSF Chimera—a visualization system for exploratory research and analysis. *J. Comput. Chem.* **25**, 1605–1612 (2004).
49. Emsley, P. & Cowtan, K. Coot: model-building tools for molecular graphics. *Acta Crystallogr. D* **60**, 2126–2132 (2004).
50. Adams, P. D. et al. PHENIX: a comprehensive Python-based system for macromolecular structure solution. *Acta Crystallogr. D* **66**, 213–221 (2010).
51. Ha, K. S., Touloukhonov, I., Vassilyev, D. G. & Landick, R. The NusA N-terminal domain is necessary and sufficient for enhancement of transcriptional pausing via interaction with the RNA exit channel of RNA polymerase. *J. Mol. Biol.* **401**, 708–725 (2010).
52. Chakraborty, A. et al. Opening and closing of the bacterial RNA polymerase clamp. *Science* **337**, 591–595 (2012).
53. Feklistov, A. et al. RNA polymerase motions during promoter melting. *Science* **356**, 863–866 (2017).

**Acknowledgements** The work was supported by Strategic Priority Research Program of the CAS XDB29020000 (Y. Zhang), National Key Research and Development Program of China 2018YFA0903701 (Y. Zhang), Basic Research Zone Program of Shanghai JCYJ-SHFY-2022-012 (Y. Zhang), Shanghai Science and Technology Innovation program (19JC1415900) (Y. Zhang), and US National Institute of General Medical Sciences, NIH (GM38660) (R.L.). We thank L. Kong, F. Wang, G. Li and J. Duan at the Cryo-EM Center of NFPS in Shanghai and S. Chang at the Cryo-EM Center of Zhejiang University for assistance in cryo-EM data collection.

**Author contributions** L.Y. collected the cryo-EM data and solved the cryo-EM structures. L.Y., E.O.O., C.Y. and R.A.M. designed, performed and analysed biochemical experiments. J.S., L.S., X.W., A.W., D.H., Y. Zeng and Y.F. assisted in structure determination. R.L. and Y. Zhang designed experiments, analysed data and wrote the manuscript.

**Competing interests** The authors declare no competing interests.

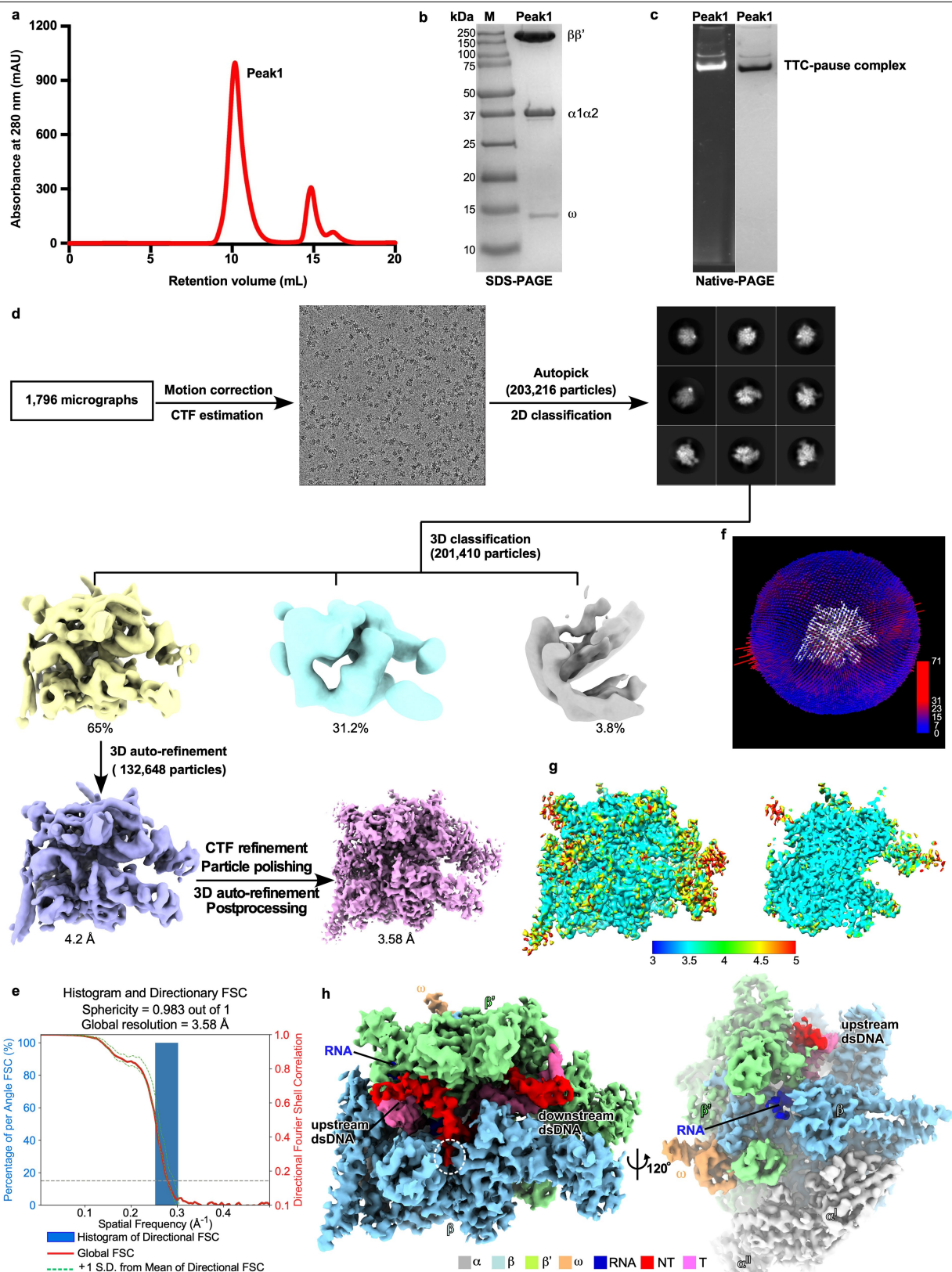
**Additional information**

**Supplementary information** The online version contains supplementary material available at <https://doi.org/10.1038/s41586-022-05604-1>.

**Correspondence and requests for materials** should be addressed to Yu Feng, Robert Landick or Yu Zhang.

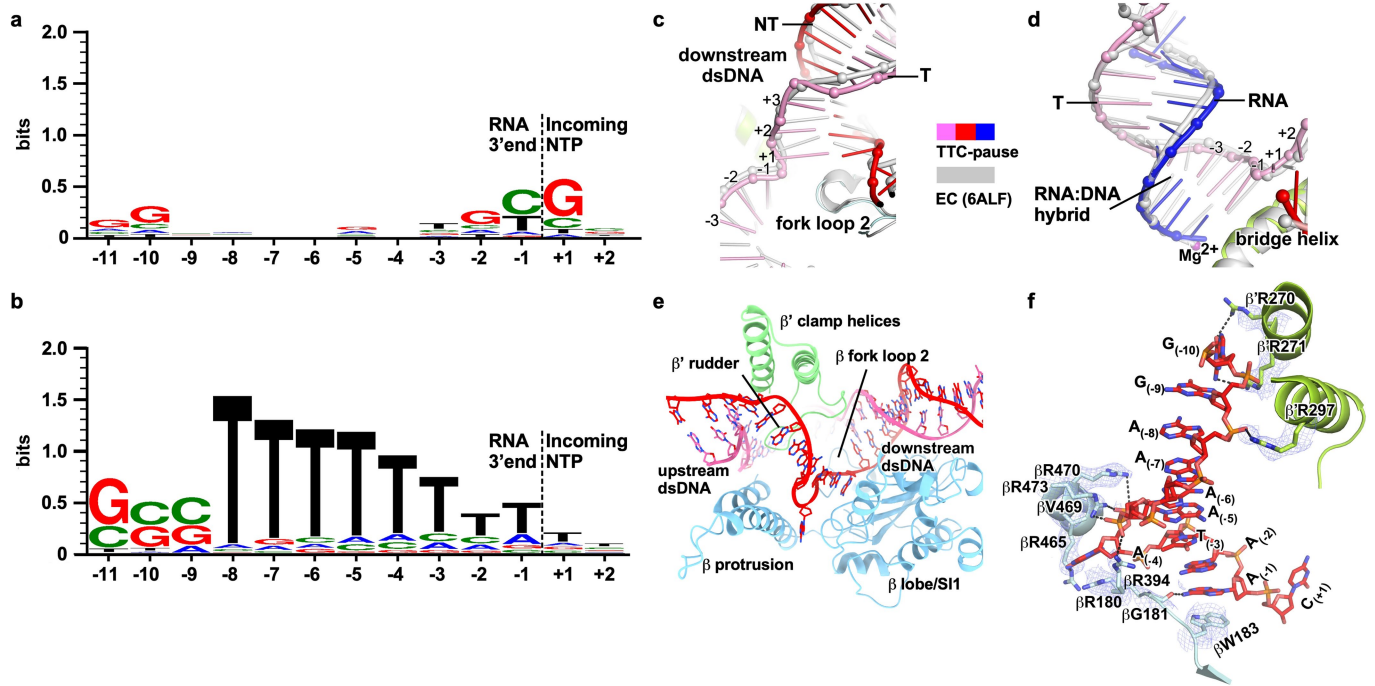
**Peer review information** Nature thanks the anonymous reviewer(s) for their contribution to the peer review of this work. Peer review reports are available.

**Reprints and permissions information** is available at <http://www.nature.com/reprints>.



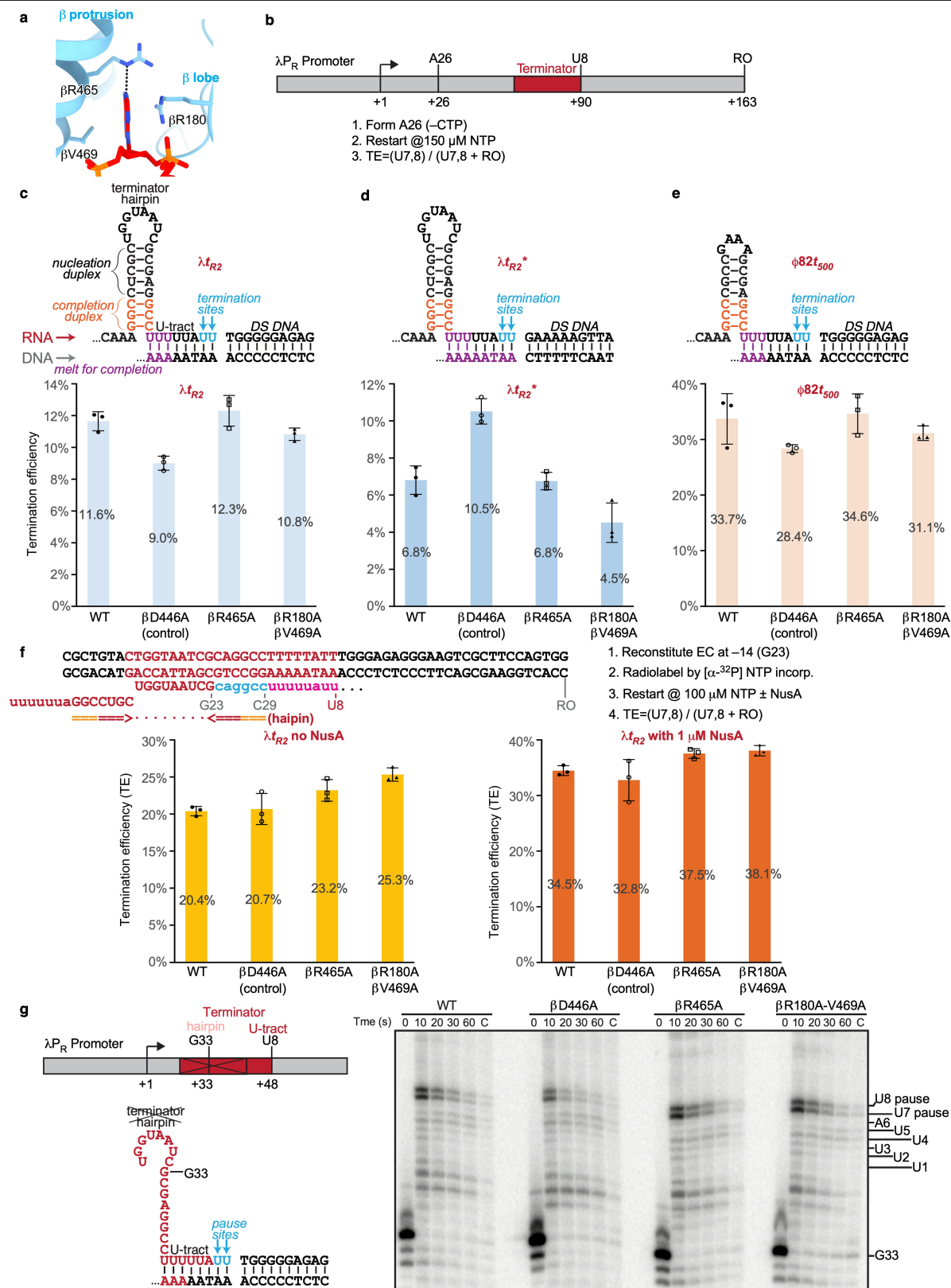
**Extended Data Fig. 1 | The processing pipeline for single-particle reconstruction of *E. coli* TTC-pause.** **a.** Elution peaks of TTC pause (peak1) from a size-exclusion column. **b.** The SDS-PAGE and **c.** the native-PAGE of peak 1. The gel was first stained with SYBR Gold for nucleic acids and then with Coomassie Brilliant Blue for proteins. The experiment has been repeated three

times with similar results. **d.** The flowchart of data processing of TTC pause. **e.** The 3D FSC plot. The dotted line represents 0.143 cutoff of the global FSC curve. **f.** The angular distribution of single-particle projections by number of particles of each projection. **g.** The cryo-EM map of TTC pause colored by local resolution. **h.** The cryo-EM map of TTC pause in front and side views.



**Extended Data Fig. 2 | The detailed analysis of TTC-pause structure.** **a.** The previously determined consensus sequence for elemental pause sites<sup>18</sup>. **b.** The consensus sequence features from 100 previously identified *E. coli* intrinsic terminators<sup>11</sup>. **c.** The structural comparison of downstream dsDNA between TTC pause (pink and red) and TEC (gray). **d.** The structural comparison of

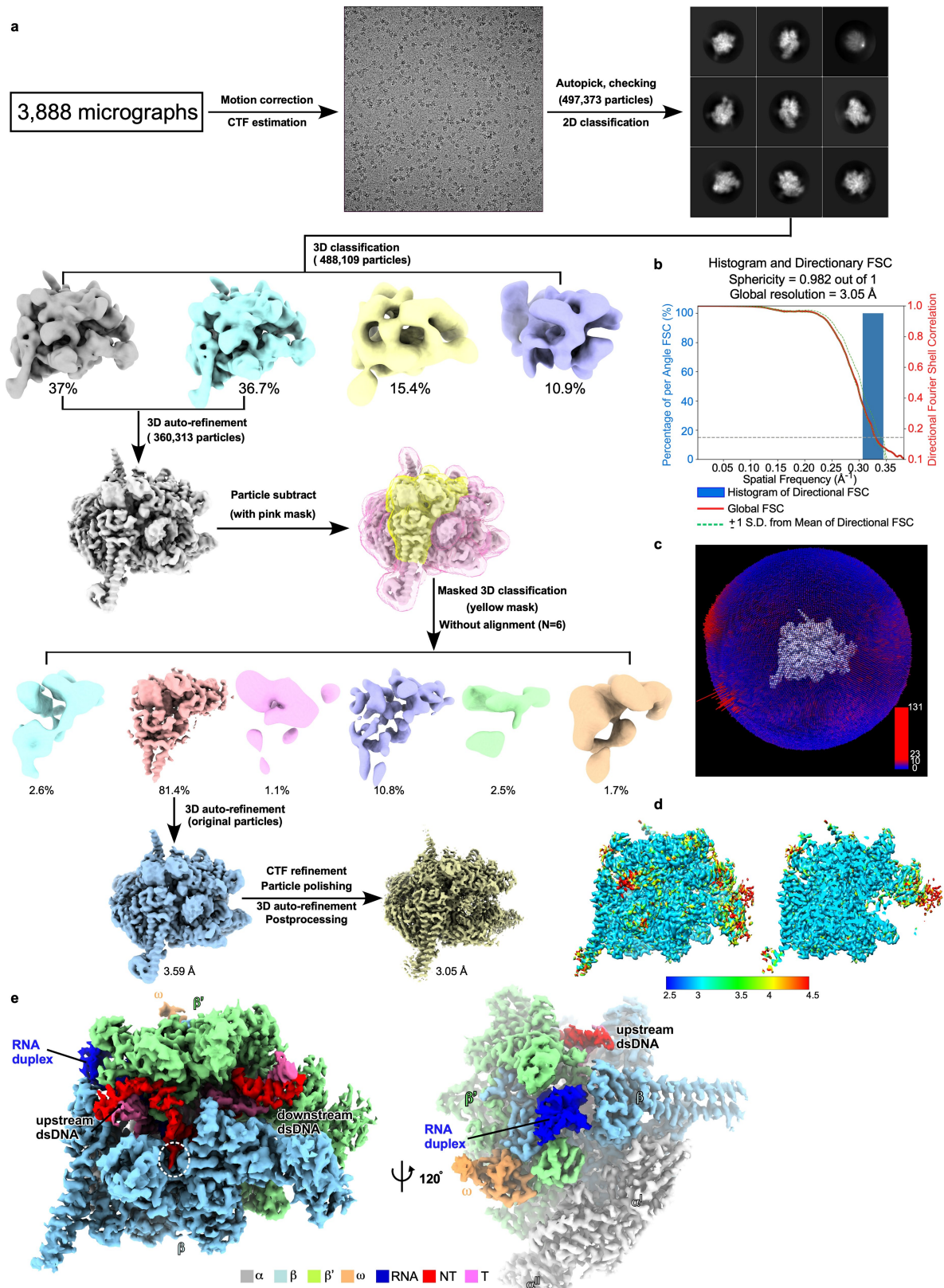
RNA-DNA hybrid between TTC pause (pink and red) and TEC (gray). **e.** The path of single-stranded ntDNA of the transcription bubble in RNAP. **f.** The detailed interactions between single-stranded ntDNA of the transcription bubble and RNAP. Blue mesh, the cryo-EM map. Black dash, H-bond.



Extended Data Fig. 3 | See next page for caption.

**Extended Data Fig. 3 | Disruption of NT -4 pocket interaction does not affect termination efficiency or pre-termination pausing.** **a.** NT -4 pocket with R180, R465 and V469 shown as sticks. An adenine on the non-template DNA is flipped into the pocket and hydrogen bonds with R465. **b.** DNA template encoding  $\lambda P_R$  promoter and  $\lambda t_{R2}$  terminator used for promoter-initiated, *in vitro* transcription assay of the effects of pocket mutants on termination. **c.** Effect of pocket mutants on the termination efficiency of wild-type  $\lambda t_{R2}$  terminator. **d.** Effect of pocket mutants on the termination efficiency of a  $\lambda t_{R2}$  terminator containing a different downstream DNA. **e.** Effect of pocket mutants on the termination efficiency of  $\phi 82 t_{500}$  terminator. **f.** Effect of pocket mutants on the

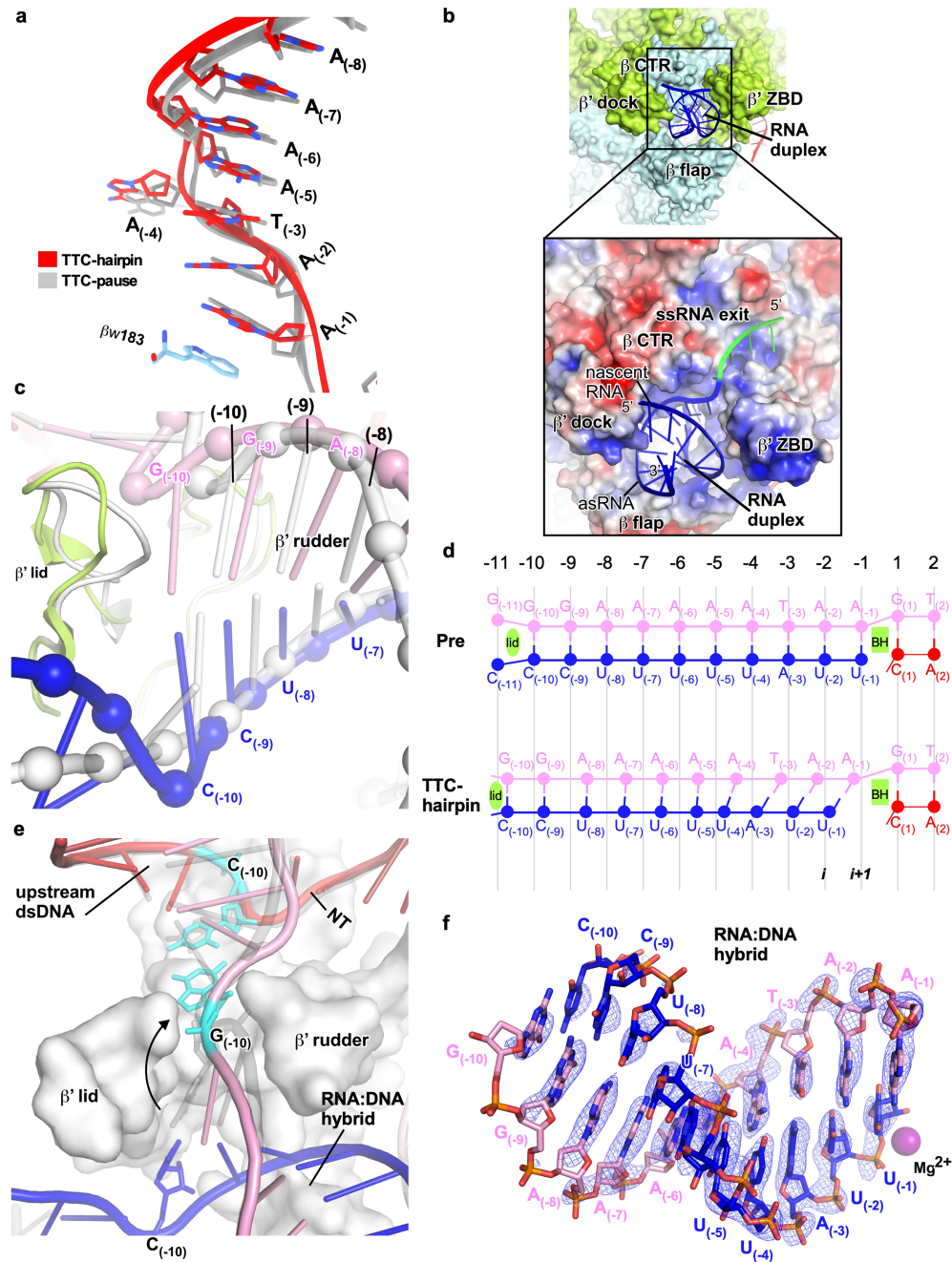
termination efficiency of a scaffold-based  $\lambda t_{R2}$  terminator in the absence or presence of *E. coli* NusA. Data are presented as mean  $\pm$  SD, n = 3 biologically independent experiments for c-f. **g.** Effect of pocket mutants on pre-termination pausing at U7 and U8. A variant of  $\lambda t_{R2}$  terminator lacking the upstream half of the terminator hairpin (pRM1234; Supplementary Table 1) and an antisense DNA to prevent backtracking of G33 complexes were used. See legend to Extended Data Fig. 8c and methods for more details. Results from a single replicate are shown. Raw data for the gels in this figure can be found in Supplementary Fig. 1a-d.



**Extended Data Fig. 4 | The complex assembly and processing pipeline for cryo-EM map construction of TTC hairpin. a.** The flowchart of data processing of TTC hairpin. **b.** The 3D FSC plot. The dotted line represents 0.143 cutoff of the global FSC curve. **c.** The angular distribution of single-particle

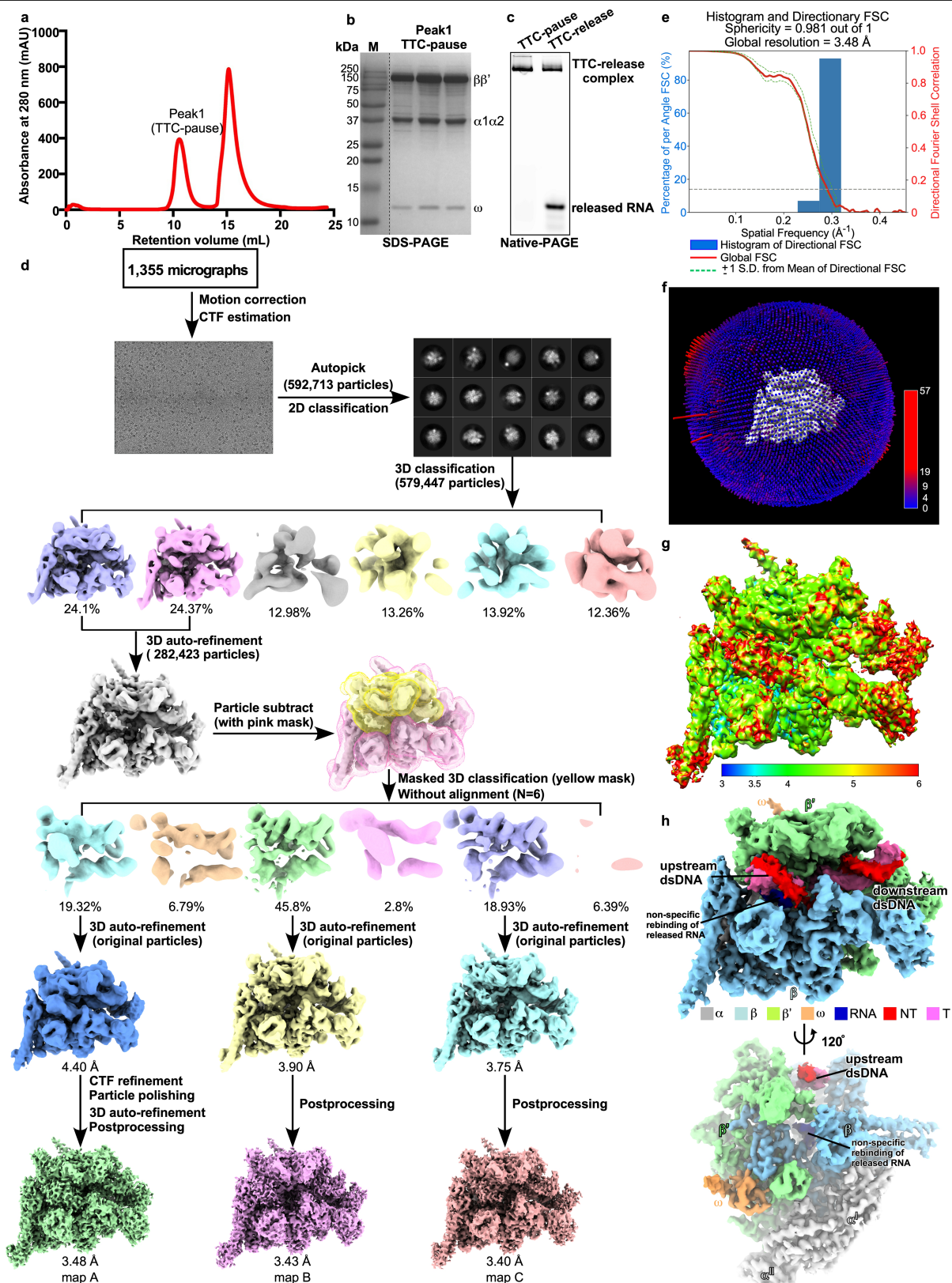
projections by number of particles of each projection. **d.** The cryo-EM map colored by local resolution. **e.** The cryo-EM map of TTC hairpin in front and side views.





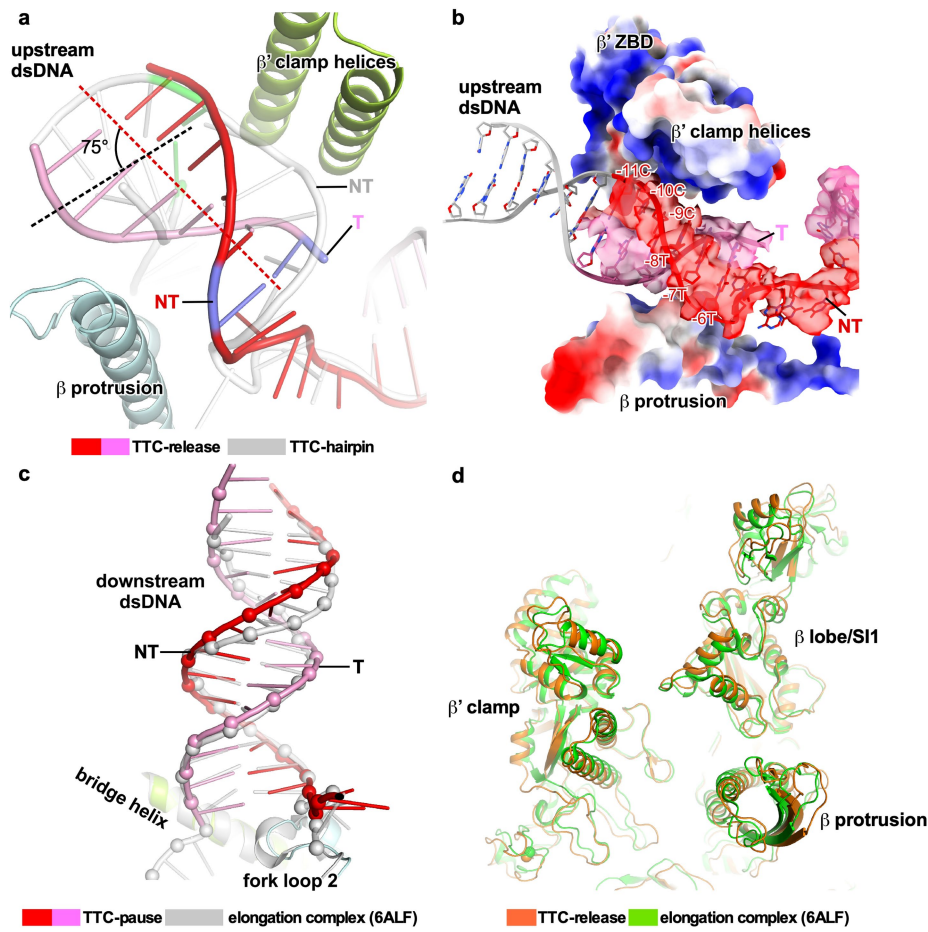
**Extended Data Fig. 5 | The detailed analysis of TTC-hairpin structure.** **a.** The comparison of nucleic acid scaffolds in TTC hairpin (red) and TTC pause (gray). **b.** A clear path across the cleft between  $\beta$  CTR and  $\beta'$  ZBD for the 5'-end ssRNA that leads into the bottom of the RNA exit channel. The insert shows a positively charged groove that likely guides 5'-proximal ssRNA upstream of the hairpin stem out of the RNA exit channel. The modeled 5'-proximal ssRNA is shown in green. The electrostatic potential surface of RNAP was generated using APBS tools in Pymol. **c.** Structural comparison of the upstream RNA-DNA hybrids in

TTC hairpin (blue and pink) and TEC (gray; PDB: 6ALF). The two structures were superimposed based on the RNAP- $\beta'$  rudder and lid motifs. **d.** The schematic presentation of the register of the RNA-DNA hybrid in TTC hairpin and a TEC in a pre-translocation state. **e.**  $G_{(-10)}$  of the tDNA (cyan) is modeled to flip from its previous position (gray) through the tunnel to pair with the  $C_{(-10)}$  of the ntDNA. **f.** The cryo-EM map shows that the -10 base pair has the weakest signal in the RNA-DNA hybrid.



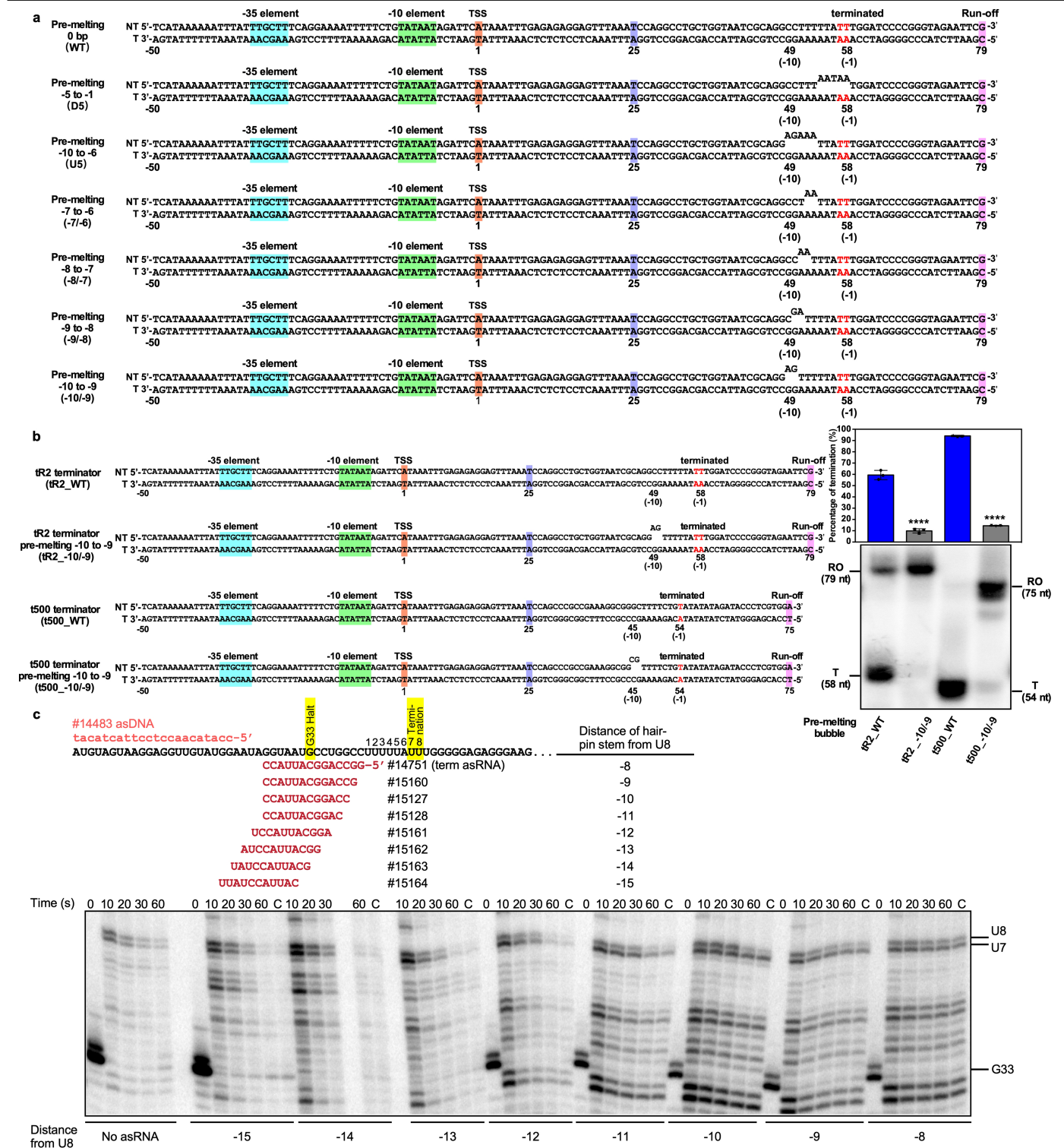
**Extended Data Fig. 6 | The complex assembly and processing pipeline for cryo-EM map construction of TTC release.** **a.** Elution peaks of TTC pause (peak1) from a size-exclusion column. **b.** The SDS-PAGE of TTC-pause. **c.** The native-PAGE of TTC pause and TTC release. The gel was visualized by Cy5-fluorescein labeled at the 5' terminus of the nascent RNA. **d.** The flowchart

of data processing of TTC release. **e.** The 3D FSC plot. The dotted line represents 0.143 cutoff of the global FSC curve. **f.** The angular distribution of single-particle projections by number of particles of each projection of map A. **g.** The map A colored by local resolution. **h.** The cryo-EM map of TTC release in front and side views.



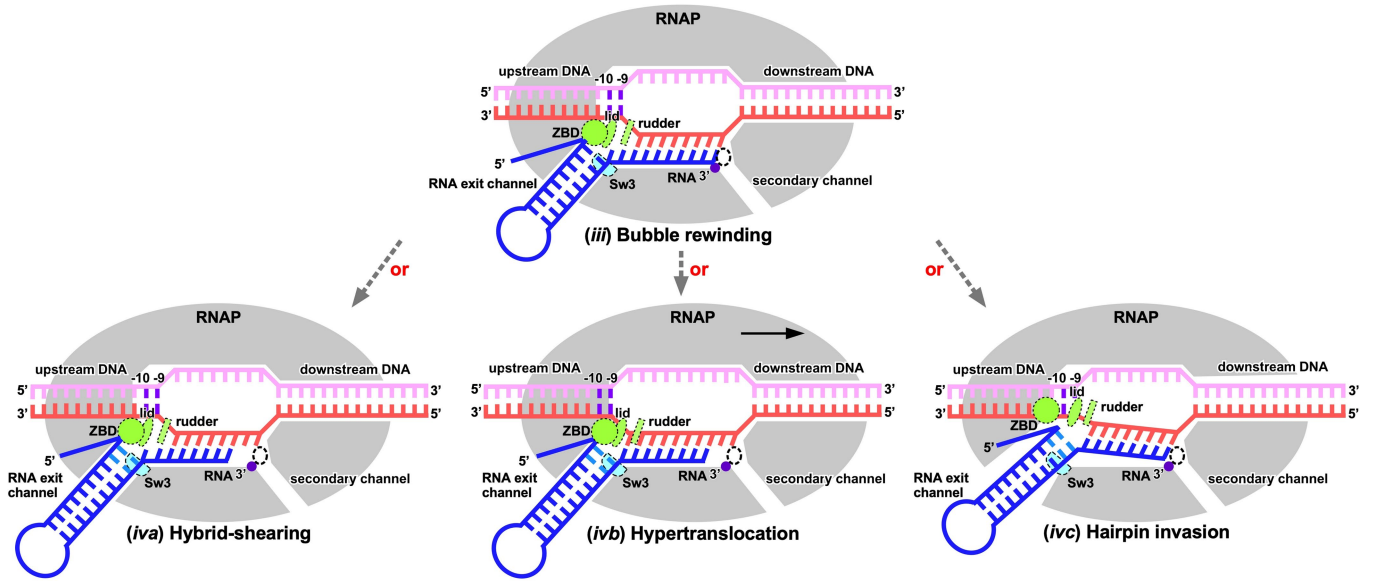
**Extended Data Fig. 7 | The detailed analysis of the TTC-release structure.**  
**a.** The comparison of upstream dsDNA in TTC release (pink and red) and TTC hairpin (gray). The last base pair of the upstream DNA in TTC release and TTC hairpin was colored as blue and green, respectively. The dashes indicate helical axis of the upstream DNA of the two structures. **b.** The modeled

upstream base pairs (-17 to -12; gray) show loss of contact with RNAP and explain loss of cryo-EM map signals in TTC release. The map and model of the upstream DNA in TTC release are shown in red and pink. **c.** The comparison of downstream dsDNA in TTC release (pink and red) and TEC (gray; PDB: 6ALF). **d.** The comparison of main cleft in TTC release (brown) and TEC (green).



**Extended Data Fig. 8 | Rewinding of transcription bubble triggers RNA release. a.** The sequence of DNA templates used in Fig. 3g. **b.** The *in vitro* transcription assay suggests that dsDNA rewinding is required for intrinsic termination at the  $\phi$ 82<sub>t500</sub> terminator. Data are presented as mean  $\pm$  SD, n = 3 biologically independent experiments, \*\*\*\*P < 0.0001; two-tailed unpaired t-tests. Raw data for the gels can be found in Supplementary Fig. 1g. **c.** Mapping the hairpin stem distance from U8 that triggers termination at U7 or U8. A template encoding a variant of  $\lambda$ t<sub>R2</sub> terminator lacking the upstream half of the terminator hairpin was used (from pRM1234, Supplementary Table 1).

Core-RNAP was halted at G33, and backtracking was prevented by addition of asDNA (#14483). Transcription was restarted after adding different asRNAs and a master mix with (ATP + GTP + CTP to yield final concentrations of 150  $\mu$ M, and UTP to 10  $\mu$ M). Samples were collected and mixed with stop buffer after 10, 20, 30, and 60 sec. The remaining fraction was then chased by all 4 NTPs to a final concentration of 650  $\mu$ M each. Termination starts taking place when the hairpin is -11 away from U8. Results from a single replicate are shown. Raw data for the gel can be found in Supplementary Fig. 1h.



**Extended Data Fig. 9 | The proposed pathways of hairpin extension after the TTC-hairpin intermediate.** The choice between the alternative pathways of hybrid-shearing and hypertranslocation depends on terminator sequences<sup>26</sup>. It is also possible that hairpin completion follows a third alternative pathway, 'hairpin invasion'<sup>12,25,28,36</sup>, in which the RNAP clamp opens to allow hairpin extension into the main cleft. Although clamp opening cannot be obligatory for

RNA release<sup>30</sup>, the RNAP clamp is in constant thermal motion<sup>52,53</sup>, can open fully in some conditions<sup>36-39</sup>, and thus in principle could open upon DNA rewinding and allow the hairpin stem to extend into the main cleft without steric hinderance. After hairpin extension aided by bubble collapse, RNA release leads to TTC release (see Fig. 4).

	<b>TTC-pause (EMDB-33996) (PDB 7YP9)</b>	<b>TTC-hairpin (EMDB-33997) (PDB 7YPA)</b>	<b>TTC-release (EMDB-33998) (PDB 7YPB)</b>
<b>Data collection and processing</b>			
Magnification	22,500	22,500	64,000
Voltage (kV)	300	300	300
Electron exposure (e <sup>-</sup> /Å <sup>2</sup> )	60.8	58.5	49.6
Defocus range (μm)	-1.2 to -2.2	-1.8 to -2.6	-1.2 to -2.2
Pixel size (Å)	1.0	1.307	1.1
Symmetry imposed	C1	C1	C1
Initial particle images (no.)	203,216	497,373	592,713
Final particle images (no.)	132,648	294,721	54,471
Map resolution (Å)	3.58	3.05	3.48
FSC threshold	0.143	0.143	0.143
Map resolution range (Å)	3-5	2.5-4.5	3-6
<b>Refinement</b>			
Initial model used (PDB code)	6ALF	6ASX	6ASX
Model resolution (Å)	3.5	3.0	3.4
FSC threshold	0.143	0.143	0.143
Model resolution range (Å)	3-5	2.5-4.5	3-6
Map sharpening <i>B</i> factor (Å <sup>2</sup> )	-112.57	-59.23	-90.8
<b>Model composition</b>			
Non-hydrogen atoms	24,548	26,022	25,626
Protein residues	3,013	3,129	3,133
Ligands	2/1	2/1	2/1
<b><i>B</i> factors (Å<sup>2</sup>)</b>			
Protein	35.89	43.66	31.81
Nucleotide	56.84	110.2	113.78
Ligand	52.73	63.86	49.7
<b>R.m.s. deviations</b>			
Bond lengths (Å)	0.003	0.003	0.002
Bond angles (°)	0.674	0.575	0.556
<b>Validation</b>			
MolProbity score	1.52	1.27	1.23
Clashscore	5.57	3.02	2.96
Poor rotamers (%)	0.08	0.08	0.04
<b>Ramachandran plot</b>			
Favored (%)	96.56	96.94	97.23
Allowed (%)	3.44	3.06	2.77
Disallowed (%)	0	0	0

## Reporting Summary

Nature Portfolio wishes to improve the reproducibility of the work that we publish. This form provides structure for consistency and transparency in reporting. For further information on Nature Portfolio policies, see our [Editorial Policies](#) and the [Editorial Policy Checklist](#).

### Statistics

For all statistical analyses, confirm that the following items are present in the figure legend, table legend, main text, or Methods section.

- | n/a                                 | Confirmed  |
|-------------------------------------|--|
| <input type="checkbox"/>            | <input checked="" type="checkbox"/> The exact sample size ( $n$ ) for each experimental group/condition, given as a discrete number and unit of measurement  |
| <input type="checkbox"/>            | <input checked="" type="checkbox"/> A statement on whether measurements were taken from distinct samples or whether the same sample was measured repeatedly  |
| <input type="checkbox"/>            | <input checked="" type="checkbox"/> The statistical test(s) used AND whether they are one- or two-sided<br><i>Only common tests should be described solely by name; describe more complex techniques in the Methods section.</i>   |
| <input checked="" type="checkbox"/> | <input type="checkbox"/> A description of all covariates tested  |
| <input checked="" type="checkbox"/> | <input type="checkbox"/> A description of any assumptions or corrections, such as tests of normality and adjustment for multiple comparisons   |
| <input type="checkbox"/>            | <input checked="" type="checkbox"/> A full description of the statistical parameters including central tendency (e.g. means) or other basic estimates (e.g. regression coefficient) AND variation (e.g. standard deviation) or associated estimates of uncertainty (e.g. confidence intervals) |
| <input type="checkbox"/>            | <input checked="" type="checkbox"/> For null hypothesis testing, the test statistic (e.g. $F$ , $t$ , $r$ ) with confidence intervals, effect sizes, degrees of freedom and $P$ value noted<br><i>Give <math>P</math> values as exact values whenever suitable.</i>                            |
| <input checked="" type="checkbox"/> | <input type="checkbox"/> For Bayesian analysis, information on the choice of priors and Markov chain Monte Carlo settings  |
| <input checked="" type="checkbox"/> | <input type="checkbox"/> For hierarchical and complex designs, identification of the appropriate level for tests and full reporting of outcomes  |
| <input checked="" type="checkbox"/> | <input type="checkbox"/> Estimates of effect sizes (e.g. Cohen's $d$ , Pearson's $r$ ), indicating how they were calculated  |

*Our web collection on [statistics for biologists](#) contains articles on many of the points above.*

### Software and code

Policy information about [availability of computer code](#)

Data collection

The SerialEM (version 3.8) was used to collect the cryo-EM micrographs.  
The EPU (version 2.12) was used to collect the cryo-EM micrographs.

Data analysis

MotionCor2, CTFIND4, and RELION 3.08 were used to process cryo-EM single particles.  
Phenix (version 1.14-3260-000) was used to perform structure refinement.  
Coot (version 0.8.9.2) was used to perform structure model building.  
UCSF Chimera (version 1.14) was used for structure analysis.  
Typhoon (AMERSHAM TYPHOON version 5), Prism (version 9.3.1), Image J (version 1.53a), and KaleidaGraph (version 5.0) were used to analysis in vitro transcription data, release assay.  
UCSF ChimeraX (version 1.3) and PyMOL (version 2.1) were used to prepare figures and videos.

For manuscripts utilizing custom algorithms or software that are central to the research but not yet described in published literature, software must be made available to editors and reviewers. We strongly encourage code deposition in a community repository (e.g. GitHub). See the Nature Portfolio [guidelines for submitting code & software](#) for further information.

## Data

Policy information about [availability of data](#)

All manuscripts must include a [data availability statement](#). This statement should provide the following information, where applicable:

- Accession codes, unique identifiers, or web links for publicly available datasets
- A description of any restrictions on data availability
- For clinical datasets or third party data, please ensure that the statement adheres to our [policy](#)

The cryo-EM map and coordinates were deposited in Protein Data Bank and Electron Microscopy Data Bank (TTC-pause: 7YP9 and EMD-33996; TTC-hairpin: 7YPA, EMD-33997; TTC-release: 7YPB, EMD-33998)

## Human research participants

Policy information about [studies involving human research participants and Sex and Gender in Research](#).

Reporting on sex and gender

N/A

Population characteristics

N/A

Recruitment

N/A

Ethics oversight

N/A

Note that full information on the approval of the study protocol must also be provided in the manuscript.

## Field-specific reporting

Please select the one below that is the best fit for your research. If you are not sure, read the appropriate sections before making your selection.

Life sciences       Behavioural & social sciences       Ecological, evolutionary & environmental sciences

For a reference copy of the document with all sections, see [nature.com/documents/nr-reporting-summary-flat.pdf](https://www.nature.com/documents/nr-reporting-summary-flat.pdf)

## Life sciences study design

All studies must disclose on these points even when the disclosure is negative.

Sample size

The sample size has been described in the figure legends. No statistical method has been used to predetermine the sample size. Experiments were typically repeated in triplicates independently to ensure the robustness of conclusions.

Data exclusions

No data was excluded.

Replication

The replicate numbers for each experiments were described in the respective figure legends. Experiments were typically repeated in triplicates independently to ensure the robustness of conclusions. All attempts at replication were successful.

Randomization

Not applicable as no groups to be allocated.

Blinding

Not applicable as no groups to be allocated.

## Reporting for specific materials, systems and methods

We require information from authors about some types of materials, experimental systems and methods used in many studies. Here, indicate whether each material, system or method listed is relevant to your study. If you are not sure if a list item applies to your research, read the appropriate section before selecting a response.



## Materials & experimental systems

- | n/a                                 | Included in the study                                  |
|-------------------------------------|--|
| <input checked="" type="checkbox"/> | <input type="checkbox"/> Antibodies                    |
| <input checked="" type="checkbox"/> | <input type="checkbox"/> Eukaryotic cell lines         |
| <input checked="" type="checkbox"/> | <input type="checkbox"/> Palaeontology and archaeology |
| <input checked="" type="checkbox"/> | <input type="checkbox"/> Animals and other organisms   |
| <input checked="" type="checkbox"/> | <input type="checkbox"/> Clinical data                 |
| <input checked="" type="checkbox"/> | <input type="checkbox"/> Dual use research of concern  |

## Methods

- | n/a                                 | Included in the study                           |
|-------------------------------------|---|
| <input checked="" type="checkbox"/> | <input type="checkbox"/> ChIP-seq               |
| <input checked="" type="checkbox"/> | <input type="checkbox"/> Flow cytometry         |
| <input checked="" type="checkbox"/> | <input type="checkbox"/> MRI-based neuroimaging |